TECHNISCHE UNIVERSITÄT WIEN

INSTITUTE FOR THEORETICAL PHYSICS

DIPLOMARBEIT

Single-Photon Transfer in a Dispersion-Engineered Chiral Waveguide

zur Erlangung des akademischen Grades

Diplom-Ingenieur

im Rahmen des Studiums

Technische Physik

eingereicht von

Lorenz Fischer, BSc
Matrikelnummer 11811349

ausgeführt am Institut für Theoretische Physik
der Fakultät für Physik der Technischen Universität Wien

Betreuung
Betreuer: Ass. Prof. Dr. Carlos Gonzalez-Ballestero
Mitwirkung: Univ.Prof. Dipl.-Ing. Dr.techn. Stefan Rotter

Wien, 29.08.2024

(Unterschrift Verfasser) (Unterschrift Betreuer)

Contents

Acknowledgments

Firstly, I want to thank Prof. Stefan Rotter for giving me the opportunity to work on my diploma project and kindly welcoming me to his working group. I want to express my deepest gratitude to my supervisors Dr. Carlos Gonzalez-Ballestero and Oliver Diekmann for their advice, ongoing support and enthusiasm for this project. They always had an open ear for my questions and took the time to discuss the physics and numerics. I also want to thank the whole working group for the great atmosphere, the interesting (lunch) discussions and simply making my time spent at the institute during my diploma project very enjoyable. Additionally, I want to thank Julian Köberle, David Fürlinger and Patrick Kraus for great discussions about physics and everything else. Furthermore, I want to express my gratitude to all other colleagues, who accompanied me through the years of my physics studies at TU Wien. Finally, I want to thank my family and friends for their ongoing support, encouragement and patience during my studies.

Abstract

The perfect transfer of single photons in quantum systems is crucial for advancing quantum information and quantum communication technologies. Chiral waveguide quantum electrodynamics (QED) setups serve as promising platforms in this context. In chiral one-dimensional (1D) waveguides, photon emission becomes unidirectional due to the spin-orbit interaction of light. In principle, this would allow a qubit to emit a photon with unit probability towards a second qubit, increasing the probability of absorption by the latter. However, with a linear dispersion relation in the chiral waveguide, single-photon absorption is fundamentally limited to about 54% due to the constraints on the shape of the single-photon pulse governed by the time-reversal symmetry of the Schrödinger equation. In the literature, these constraints on the pulse shape for efficient absorption have been overcome by using cavities, spectrally engineering the couplings or modeling time-dependent couplings.

In this thesis, we explore an alternative approach, namely to engineer the dispersion relation of the chiral waveguide such that the single-photon pulse is reshaped, just by free propagation in the waveguide, to enhance its absorption. Specifically, we investigate a system of two identical qubits, which are chirally coupled to a 1D photonic waveguide. By numerical optimization, we find the dispersion relation that maximizes the absorption of a spontaneously emitted photon by the second qubit. In the optimization, the absorption is maximized by optimizing the spatial overlap between the propagating single-photon pulse, which is deformed according to the dispersion relation, and the time-reversed initial pulse. All calculations and numerical simulations are carried out under the Markov approximation. The results are verified by exact diagonalization. We demonstrate that by engineering the dispersion relation in a chiral waveguide, the single-photon transfer is improved compared to a linear dispersion relation. Additionally, our work suggests that exploring the non-Markovian regime is necessary to further enhance the single-photon transfer efficiency.

Kurzfassung

Der perfekte Transfer von einzelnen Photonen in Quantensystemen ist entscheidend für die Weiterentwicklung von Quanteninformations- und Quantenkommunikationstechnologien. Chirale Wellenleiter-Quantenelektrodynamik (QED) stellt eine vielversprechende Plattform in diesem Kontext dar. In chiralen eindimensionalen (1D) Wellenleitern wird die Photonenemission aufgrund der Spin-Orbit Wechselwirkung von Licht unidirektional. Im Prinzip würde dies einem Qubit ermöglichen, ein Photon mit Wahrscheinlichkeit eins in Richtung eines zweiten Qubits zu emittieren, was zu einer erhöhten Wahrscheinlichkeit der Absorption durch letzteres führt. In einem chiralen Wellenleiter mit linearer Dispersion ist die Absorption von einzelnen Photonen jedoch fundamental limitiert bei etwa 54%, aufgrund der Einschränkungen der Form des Einzelphotonenpulses durch die Zeitumkehrsymmetrie der Schrödingergleichung. In der Literatur wurden diese Einschränkungen der Pulsform für effiziente Absorption mittels Hohlraumresonatoren, spektraler Modifizierung der Kopplungen oder Modellierung von zeitabhängigen Kopplungen überwunden.

In dieser Arbeit untersuchen wir eine alternative Methode, nämlich die Dispersionsrelation des chiralen Wellenleiters so zu konstruieren, dass der Einzelphotonenpuls nur durch die freie Propagation im Wellenleiter deformiert wird, um seine Absorption zu verbessern. Konkret untersuchen wir ein System aus zwei identischen Qubits, welche chiral an einen 1D Wellenleiter gekoppelt sind. Durch numerische Optimierung erhalten wir jene Dispersionsrelation, welche die Absorption eines spontan emittierten Photons durch das zweite Qubit maximiert. In der Optimierung wird die Absorption maximiert, indem der räumliche Überlapp zwischen dem propagierenden Puls, welcher aufgrund der Dispersionsrelation deformiert wird, und dem zeitumgekehrten ursprünglich emittierten Puls optimiert wird. Alle Rechnungen und numerische Simulationen werden unter der Markov-Approximation ausgeführt. Die Resultate werden durch exakte Diagonalisierung verifiziert. Wir zeigen, dass durch die Konstruktion der Dispersionsrelation in einem chiralen Wellenleiter der Transfer von einzelnen Photonen im Vergleich zu einer linearen Dispersionsrelation verbessert wird. Zusätzlich legt unsere Arbeit nahe, dass die Untersuchung des nicht-Markov'schen Regimes notwendig ist, um die Effizienz des Transports von einzelnen Photonen weiter zu erhöhen.

1 Introduction

"If I have seen further, it is by standing on the shoulders of giants."

— Isaac Newton, *letter to Robert Hooke, 1675*

The interaction of a single photon with a single quantum emitter (e.g. a qubit) is the most fundamental building block of quantum optics [1]. An important goal is to develop techniques for the control of such light-matter interactions at the level of single quanta, which enables many applications, e.g. in the fields of quantum communication and quantum information [2]. By achieving perfect absorption of a single photon by a single qubit, it may be possible to build quantum networks where quantum information is transferred between different nodes via photons in quantum channels (e.g. optical fibers) [3]. Quantum networks play an important role in the theoretical understanding and the physical implementation of quantum computing and communication [3]. This motivates the research on quantum systems which could realize such quantum networks. In this context, it is usually necessary to spatially confine the electromagnetic field in order to increase the qubit-light coupling rate, which is too weak in free space. Two popular alternatives to achieve this are cavity quantum electrodynamics (QED), where qubits are coupled to a single mode [4–7] or multiple discrete modes [8], and waveguide QED, where qubits are coupled to a one-dimensional (1D) continuum of modes [9–12]. Waveguides are well suited for large-scale quantum information applications because they allow for easy in- and out-coupling of information. On the other hand, because a photon emitted by a qubit into an open waveguide has an equal probability of traveling in either direction, the probability that a qubit at one of the waveguide arms absorbs the photon is fundamentally limited by 50% (the limit is even stricter due to time-reversal symmetry, as we discuss below). This makes perfect transfer of a single photon impossible.

In recent years, chiral waveguides have emerged as an exciting new approach to quantum control of light-matter interactions [13, 14]. In chiral 1D waveguides, an emitted photon can be channeled into one of the two propagation directions due to the spin-orbit interaction of light [15]. In principle, this would allow a qubit to emit a photon with unit probability towards a second qubit, increasing the probability of absorption by the latter. Experiments have already shown strong unidirectional photon emission from nanoparticles and qubit ensembles in dielectric waveguides [15, 16] as well as from quantum dots in photonic crystals [17–19]. By taking an ensemble of quantum emitters chirally coupled to

a 1D waveguide, interesting quantum many-body effects come into play, such as modified superradiance [20]. With this, it may be possible to realize a cascaded quantum system [21], in which photons can be transported along a chain of qubits without information backflow.

Despite the increased probability of absorption due to unidirectional propagation, a single photon spontaneously emitted by a qubit into a chiral waveguide with linear dispersion relation, $\omega(k) = ck$, still cannot be perfectly absorbed by a second qubit. Indeed, the absorption probability of the second qubit, defined as the occupation of the second qubit as a function of time, has a maximum of $4/e^2 \approx 54\%$[1] [22]. This is because the single-photon pulse emitted by a qubit in this case has a decaying exponential envelope [23, 24] and it thus not time-reversal symmetric, which would be necessary for perfect absorption according to the time-reversal symmetry of the Schrödinger equation. The latter implies that the absorption process is the time-reversed emission process. Thus, for perfect absorption, the incident single-photon pulse needs to have the shape of the time-reversed initial photon pulse emitted by a qubit. This has been studied in free space, e.g. in Refs. [22, 25–27]. Several approaches to overcome the constraints on the pulse shape for efficient absorption have been taken in the literature. A suitable method is to modify the pulse emission, such that the emitted single-photon pulse is already time-reversal symmetric. This has been achieved by driving a qubit in a cavity [4], using spectrally engineered couplings [8] or time-dependent couplings [28]. A different approach is to time-reverse the emitted single-photon pulse by using an asymmetric cavity, as shown in Ref. [29].

Here, we explore an alternative approach, namely to engineer the dispersion relation of the waveguide such that the single-photon pulse is reshaped, just by free propagation in the waveguide, to maximize its absorption by the second qubit. More specifically, in this thesis, we study how the single-photon transfer in a chiral 1D waveguide can be improved by engineering a non-linear dispersion relation to reshape the single-photon pulse towards the time-reversed initial pulse. We investigate a system of two identical qubits, which are chirally coupled to a 1D photonic waveguide. The excitation probability of the first and second qubit is initially given by $P_1(t = 0) = 1$ and $P_2(t = 0) = 0$, respectively. Our aim is to optimize the maximum excitation probability of the second qubit, $\max_t P_2(t)$. By numerical optimization, we obtain the optimal non-linear dispersion relation, i.e. the dispersion relation which maximizes $\max_t P_2(t)$. With the engineered non-linear dispersion relation, we can reshape the single-photon pulse such that the absorption is indeed improved compared to the linear case.

This thesis is structured as follows. In Chap. 2, we introduce the theoretical framework which serves as the basis for the thesis. In this chapter, we first discuss Wigner-Weisskopf theory, the description of spontaneous photon emission. Then, we present paradigmatic calculations for a single qubit chirally coupled to a 1D waveguide. Hereby, the observables of interest, namely the emission spectrum and the single-photon pulse, are defined. This

[1] The maximum absorption of a single photon by a second qubit for a linear dispersion will be explicitly calculated in this thesis, see Sec. 3.1.2

is important in order to understand the two-qubit system. In Chap. 3, we study the single-photon transfer between two qubits in the chiral waveguide. We calculate the excitation probability of the second qubit for a linear dispersion in the chiral waveguide. This analysis shows the problem arising with a linear dispersion. To improve the single-photon absorption, we use non-linear dispersion relations to deform the single-photon pulse towards the optimal shape for absorption. Hereby, we introduce our scheme to optimize the dispersion relations, such that the spatial overlap between the single-photon pulse and its time-reversed shape is maximized. Finally, we address the verification of the results obtained with non-linear dispersion relations using exact diagonalization. In Chap. 4, we apply our method to a system of two qubits chirally coupled to a 1D waveguide. First, we discuss the results for a dispersion relation of polynomial degree $N = 3$, in particular the parameter combinations' behaviour. Following this analysis, we focus on the results for dispersion relations of higher order. The results are compared to the solutions obtained via exact diagonalization. Finally, in Chap. 5, we give a conclusion and an outlook.

2 Theoretical Framework

In this chapter, we present the underlying theoretical models and calculations, which provide the basis for this thesis. First, we discuss Wigner-Weisskopf theory, which describes the spontaneous emission of photons into free space, for our system. Then, the photon emission by a single qubit into the waveguide is discussed. Hereby, the observables of interest (emission spectrum and single-photon pulse) will be defined and calculated, where especially the form of the single-photon pulse for a linear dispersion, $\omega(k) = ck$, in the waveguide is presented. These paradigmatic calculations for a single qubit are needed to understand the two-qubit case.

2.1 Wigner-Weisskopf theory of spontaneous emission

The excited state of a qubit is not a stable state. The qubit will eventually decay to the ground state by spontaneous photon emission. The spectrum of the emitted photon is peaked around the frequency corresponding to the qubit transition. This spontaneous decay is caused by the coupling of the qubit to the QED vacuum (vacuum fluctuations). Mathematically, the decay in free space shows as an exponential decrease of the qubit excitation probability as a function of time. The original explanation of spontaneous emission goes back to Albert Einstein studying the blackbody spectrum [30]. The rate of spontaneous emission (decay rate) for the corresponding qubit transition is also known as the "Einstein A coefficient" [31]. Victor Weisskopf and Eugene Wigner later provided a description of spontaneous emission in the QED framework in their seminal paper from 1930 [32]. We will follow the Wigner-Weisskopf formalism in the following calculations.

2.1.1 Model Hamiltonian and equations of motion

In our system, identical qubits are chirally coupled to a 1D photonic waveguide (see Fig. 2.1). Although we consider the system with one or two qubits in this thesis, we keep the number of qubits general at this point. The qubits are modeled as two-level systems with transition frequency ω_q and are equally spaced with a separation of d between neighbouring qubits. We assume perfect chiral coupling, which means that an emitted photon only propagates along one direction in the waveguide, without being reflected backwards. This is modeled by taking the coupling rate between qubit and left-propagating modes to zero.

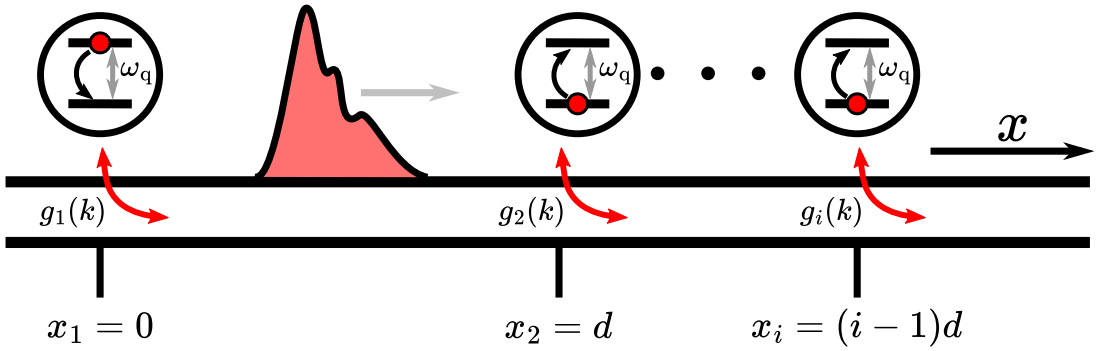

Figure 2.1: Multiple equally spaced qubits chirally coupled to a 1D photonic waveguide.

In the rotating wave approximation (RWA) the Hamiltonian reads ($\hbar = 1$)

$$H = \underbrace{\sum_i \omega_q |e_i\rangle\langle e_i|}_{\equiv H_Q} + \underbrace{\int_0^\infty dk\, \omega(k) a^\dagger(k) a(k)}_{\equiv H_F} + \underbrace{\sum_i \int_0^\infty dk\, \left[g_i(k) a(k) \sigma_i^+ + \text{h.c.}\right]}_{\equiv H_{QF}}, \tag{2.1}$$

The photonic creation and annihilation operators fulfil the commutation relation $[a(k), a^\dagger(k')] = \delta(k - k')$. The $g_i(k)$ are the couplings of the ith qubit to the modes and $\omega(k)$ is the frequency of mode k (dispersion relation). Because the Hamiltonian commutes with the excitation number, we can restrict our study to the single-excitation subspace. The wavefunction for the single-excitation subspace of the full system Hamiltonian in Eq. (2.1) can then be written for all times in the Wigner-Weisskopf form

$$|\psi(t)\rangle = \left(\sum_i c_i(t)\sigma_i^+ + \int_0^\infty dk\, c(k;t) a^\dagger(k)\right)\left(\bigotimes_j |g_j\rangle\right)|0\rangle, \tag{2.2}$$

where the states $|g_i\rangle$ and $|0\rangle$ correspond to the ith qubit in the ground state and no photons in the waveguide (vacuum state), respectively. The excited state of the ith qubit, $|e_i\rangle$, and the single-photon states, $|1_k\rangle$, are defined as $|e_i\rangle := \sigma_i^+|g_i\rangle$ and $|1_k\rangle := a^\dagger(k)|0\rangle$, respectively. The $c_i(t)$ and $c(k;t)$ are the probability amplitudes corresponding to the qubit excitation and the excitation in the photonic modes, respectively. For the amplitudes, we impose the initial conditions

$$\begin{aligned} c_1(t=0) &= 1, \\ c_i(t=0) &= 0, \quad \forall\, i \geq 2, \\ c(k;t=0) &= 0, \end{aligned} \tag{2.3}$$

which correspond to the first qubit being in the excited state, all other qubits being in the ground state and no photons being present in the field at time $t = 0$. By the time-dependent Schrödinger equation (TDSE),

$$i\partial_t |\psi(t)\rangle = H|\psi(t)\rangle, \tag{2.4}$$

we can obtain the equations of motion (EOMs) for the amplitudes $c_i(t)$ and $c(k;t)$. First, we write down the time derivative of the wave function

$$\begin{aligned}\partial_t|\psi(t)\rangle &= \left(\sum_i \dot{c}_i(t)\sigma_i^+ + \int_0^\infty \mathrm{d}k\, \dot{c}(k;t)a^\dagger(k)\right)\left(\bigotimes_j |\mathrm{g}_j\rangle\right)|0\rangle \\ &= \sum_i \dot{c}_i(t)\left(\bigotimes_{j\neq i}|\mathrm{g}_j\rangle\right)|\mathrm{e}_i\rangle|0\rangle + \int_0^\infty \mathrm{d}k\, \dot{c}(k;t)\left(\bigotimes_j |\mathrm{g}_j\rangle\right)|1_k\rangle,\end{aligned} \tag{2.5}$$

Then, we let the Hamiltonian act on the wave function. We start with the first term in the Hamiltonian [see Eq. (2.1)].

$$\begin{aligned}H_\mathrm{Q}|\psi(t)\rangle &= \left(\sum_i \omega_\mathrm{a}|\mathrm{e}_i\rangle\langle\mathrm{e}_i|\right)|\psi(t)\rangle \\ &= \sum_i \omega_\mathrm{q} c_i(t)\left(\bigotimes_{j\neq i}|\mathrm{g}_j\rangle\right)|\mathrm{e}_i\rangle|0\rangle.\end{aligned}$$

The second term in the Hamiltonian acting on the wavefunction yields

$$\begin{aligned}H_\mathrm{F}|\psi(t)\rangle &= \left(\int_0^\infty \mathrm{d}k\,\omega(k)a^\dagger(k)a(k)\right)|\psi(t)\rangle \\ &= \int_0^\infty \mathrm{d}k\,\omega(k)c(k;t)\left(\bigotimes_j|\mathrm{g}_j\rangle\right)|1_k\rangle.\end{aligned}$$

Lastly, we let the third term in the Hamiltonian act on the wavefunction, by which we obtain

$$\begin{aligned}H_\mathrm{QF}|\psi(t)\rangle &= \left(\sum_i\int_0^\infty \mathrm{d}k\,\left[g_i(k)a(k)\sigma_i^+ + \mathrm{h.c.}\right]\right)|\psi(t)\rangle \\ &= \sum_i\int_0^\infty \mathrm{d}k\, g_i^*(k)c_i(t)\left(\bigotimes_j|\mathrm{g}_j\rangle\right)|1_k\rangle \\ &\quad + \sum_i\int_0^\infty \mathrm{d}k\, g_i(k)c(k;t)\left(\bigotimes_{j\neq i}|\mathrm{g}_j\rangle\right)|\mathrm{e}_i\rangle|0\rangle.\end{aligned}$$

The TDSE [Eq. (2.4)] then becomes

$$\begin{aligned}\partial_t|\psi(t)\rangle &= -iH|\psi(t)\rangle \\ &= -i\sum_i\left(\omega_\mathrm{q}c_i(t) + \int_0^\infty \mathrm{d}k\, g_i(k)c(k;t)\right)\left(\bigotimes_{j\neq i}|\mathrm{g}_j\rangle\right)|\mathrm{e}_i\rangle|0\rangle \\ &\quad - i\int_0^\infty \mathrm{d}k\,\left(\omega(k)c(k;t) + \sum_i g_i^*(k)c_i(t)\right)\left(\bigotimes_j|\mathrm{g}_j\rangle\right)|1_k\rangle.\end{aligned} \tag{2.6}$$

By projecting onto the states, i.e. by multiplying Eq. (2.6) with $\left(\bigotimes_{j\neq n}\langle \mathrm{g}_j|\right)\langle \mathrm{e}_n|\langle 0|$ and $\left(\bigotimes_{j}\langle \mathrm{g}_j|\right)\langle 1_k|$ from the left using the time derivative of the wavefunction given in Eq. (2.5), we obtain the EOMs

$$\dot{c}_n(t) = -i\omega_{\mathrm{q}} c_n(t) - i\int_0^\infty \mathrm{d}k\, g_n(k) c(k;t), \tag{2.7}$$

$$\dot{c}(k;t) = -i\omega(k) c(k;t) - i\sum_n g_n^*(k) c_n(t). \tag{2.8}$$

These EOMs can be solved analytically for the amplitudes $c_n(t)$ and $c(k;t)$, which will be done for one and two qubits (see Secs. 2.2 and 3.1). In the following, we want to define the observables of interest, which can be calculated via the solutions for the amplitudes.

2.1.2 Emission spectrum

An important observable to study the photon emission characteristics is the emission spectrum. It is the probability density corresponding to finding the emitted photon in mode k at time t. The emission spectrum is defined as

$$S(k;t) := |c(k;t)|^2. \tag{2.9}$$

2.1.3 Single-photon pulse

Another important observable is the single-photon pulse. It is the probability density of finding the emitted photon at position x in the waveguide at time t. In order to obtain the single-photon pulse, we first define the field operators in 2$^{\mathrm{nd}}$ quantization,

$$\Psi(x) := \frac{1}{\sqrt{2\pi}}\int_{-\infty}^{+\infty} \mathrm{d}k\, e^{ikx} a(k), \tag{2.10}$$

$$\Psi^\dagger(x) := \frac{1}{\sqrt{2\pi}}\int_{-\infty}^{+\infty} \mathrm{d}k\, e^{-ikx} a^\dagger(k). \tag{2.11}$$

We note, that $\int \mathrm{d}x\, \Psi^\dagger(x)\Psi(x) = \int \mathrm{d}k\, a^\dagger(k)a(k)$, where $\Psi^\dagger(x)\Psi(x)$ corresponds to the probability density of finding a photon at position x in the waveguide. With this, we can define the single-photon pulse as the spatio-temporal distribution

$$n(x,t) := \langle \Psi^\dagger(x)\Psi(x)\rangle. \tag{2.12}$$

By inserting the general wavefunction given by Eq. (2.2), we can calculate the single-photon pulse explicitly and obtain

$$n(x,t) = \frac{1}{2\pi}\int_{-\infty}^{+\infty}\int_{-\infty}^{+\infty} \mathrm{d}k\ \mathrm{d}k'\, e^{i(k'-k)x} c^*(k;t) c(k';t). \tag{2.13}$$

The two integrals over k and k' factorise into one integral and its complex conjugate. Subsequently, we can write the single-photon pulse as

$$n(x,t) = \frac{1}{2\pi}\left|\int_{-\infty}^{+\infty} \mathrm{d}k\, e^{ikx} c(k;t)\right|^2. \tag{2.14}$$

2.2 Paradigmatic calculations for a single qubit

We now want to study the system with one qubit, which emits a photon into the 1D chiral waveguide. In this analysis, we will also calculate the single-photon pulse explicitly for the case of a linear dispersion relation, i.e. $\omega(k) = ck$. This is important in order to understand the photon emission characteristics, especially the form and the dynamics of the emitted single-photon pulse and the emission spectrum. It also serves as a basis to understanding and optimizing the single-photon absorption (see Sec. 3.3). The calculations will follow the Wigner-Weisskopf formalism.

2.2.1 Dynamics of the single-qubit system

The equations of motion (EOMs) [see Eqs. (2.7)-(2.8)] for a single qubit read

$$\dot{c}_e(t) = -i\omega_q c_e(t) - i\int_0^\infty \mathrm{d}k\, g(k) c(k;t), \tag{2.15}$$

$$\dot{c}(k;t) = -i\omega(k) c(k;t) - i g^*(k) c_e(t). \tag{2.16}$$

In order to solve the EOMs, we follow the standard method described in D. Steck, "*Quantum and Atom Optics*" ([33]), which is based on the Wigner-Weisskopf formalism. As a first step, we define the slowly varying amplitudes[1]

$$\tilde{c}_e(t) := c_e(t) e^{i\omega_q t}, \quad \tilde{c}(k;t) := c(k;t) e^{i\omega(k)t}, \tag{2.17}$$

for which Eqs. (2.15)-(2.16) take the form

$$\dot{\tilde{c}}_e(t) = -i\int_0^\infty \mathrm{d}k\, g(k) \tilde{c}(k;t) e^{-i[\omega(k)-\omega_q]t}, \tag{2.18}$$

$$\dot{\tilde{c}}(k;t) = -i g^*(k) \tilde{c}_e(t) e^{-i[\omega_q-\omega(k)]t}. \tag{2.19}$$

We can formally integrate Eq. (2.19), which yields

$$\tilde{c}(k;t) = -i g^*(k) \int_0^t \mathrm{d}t'\, \tilde{c}_e(t') e^{-i[\omega_q-\omega(k)]t'}, \tag{2.20}$$

where we have inserted the initial condition $c(k;0) = 0$ [see Eq. (2.3)]. By plugging this expression for the $\tilde{c}(k;t)$ back into Eq. (2.18), we obtain

$$\dot{\tilde{c}}_e(t) = -\int_0^\infty \mathrm{d}k\, |g(k)|^2 \int_0^t \mathrm{d}t'\, \tilde{c}_e(t') e^{-i[\omega(k)-\omega_q](t-t')}. \tag{2.21}$$

In order to obtain the amplitudes $\tilde{c}_e(t)$ and $\tilde{c}(k;t)$, this integro-differential equation has to be solved. For the calculations, we assume spectrally flat couplings around the qubit transition frequency, given by

$$g(k) = g_0\, \theta(k), \tag{2.22}$$

where $\theta(\cdot)$ denotes the Heaviside function.

[1] This is equivalent to changing to a rotating frame.

Qubit excitation probability

First, we calculate the amplitude of the qubit excitation, $\tilde{c}_e(t)$, for which we have the equation of motion [see Eq. (2.21)]

$$\begin{aligned}\dot{\tilde{c}}_e(t) &= -\int_0^\infty \mathrm{d}k\, |g(k)|^2 \int_0^t \mathrm{d}t'\, \tilde{c}_e(t') e^{-i[\omega(k)-\omega_\mathrm{q}](t-t')} \\ &= -g_0^2 \int_0^\infty \mathrm{d}k \int_0^t \mathrm{d}t'\, \tilde{c}_e(t') e^{-i[\omega(k)-\omega_\mathrm{q}](t-t')}.\end{aligned}$$

In order to solve the equation of motion for $\tilde{c}_e(t)$, we assume at this point a general non-linear dispersion relation of the form

$$\omega(k) = \omega_\mathrm{q} + c(k-k_\mathrm{q}) + P_n(k-k_\mathrm{q}), \tag{2.23}$$

where $P_n(k-k_\mathrm{q})$ is a polynomial of higher order n in $k-k_\mathrm{q}$ and k_q is the mode corresponding to the qubit transition frequency, i.e. $\omega(k_\mathrm{q}) = \omega_\mathrm{q}$, with $\omega_\mathrm{q} := ck_\mathrm{q}$. Additionally, we assume that $\omega(k) - \omega_\mathrm{q}$ has only one real root at $k = k_\mathrm{q}$ and that local extrema of $\omega(k)$ do not come too close to ω_q. The form of the dispersion relation will be explained in detail in Sec. 3.2. Also, we assume that $\tilde{c}_e(t')$ varies in time with a rate of $\Gamma \ll \omega_\mathrm{q}$. Therefore, we can make the replacement $\tilde{c}_e(t') \to \tilde{c}_e(t)$. This approximation is called a *Markov approximation*. It can be understood more intuitively when interpreting the replacement $t' \to t$ as erasing the system's memory of its past. Next, we look at the remaining integral

$$\int_0^t \mathrm{d}t'\, e^{-i[\omega(k)-\omega_\mathrm{q}](t-t')} = \frac{\sin([\omega(k)-\omega_\mathrm{q}]t)}{\omega(k)-\omega_\mathrm{q}} - i\frac{1-\cos([\omega(k)-\omega_\mathrm{q}]t)}{\omega(k)-\omega_\mathrm{q}}. \tag{2.24}$$

The integral of the first term over all k is π for $t > 0$ and for long times $t \gg \omega_\mathrm{q}^{-1}$ this term is oscillating around zero with an arbitrarily sharp peak around the resonance, $\omega(k) = \omega_\mathrm{q}$, for increasing t. The second, imaginary term is zero for $\omega(k) = \omega_\mathrm{q}$, and for large $t \gg \omega_\mathrm{q}^{-1}$ well approximated by $-i/[\omega(k)-\omega_\mathrm{q}]$ for $\omega(k) \neq \omega_\mathrm{q}$. We can thus write [34]

$$\int_0^t \mathrm{d}t'\, e^{-i[\omega(k)-\omega_\mathrm{q}](t-t')} \simeq \pi\delta(\omega(k)-\omega_\mathrm{q}) - i\mathcal{P}\left(\frac{1}{\omega(k)-\omega_\mathrm{q}}\right), \tag{2.25}$$

where $\mathcal{P}(\cdot)$ denotes the Cauchy principal value of a function. The imaginary part of the integral result in Eq. (2.25) leads to a frequency shift. It can be shown, that this correction is actually the Lamb shift. It is justified, that we can neglect this correction term, because in the experiment, we measure the real transition frequency ω_q, where the Lamb shift is already included (renormalized frequency). With this, we have

$$\begin{aligned}\dot{\tilde{c}}_e(t) &= -g_0^2 \tilde{c}_e(t) \int_0^\infty \mathrm{d}k \int_0^t \mathrm{d}t'\, e^{-i[\omega(k)-\omega_\mathrm{q}](t-t')} \\ &= -g_0^2 \tilde{c}_e(t) \int_0^\infty \mathrm{d}k\, \pi\delta(\omega(k)-\omega_\mathrm{q}).\end{aligned}$$

In order to evaluate the expression $\delta(\omega(k)-\omega_\mathrm{q})$, we use

$$\delta(f(x)) = \sum_i \frac{\delta(x-x_i)}{|f'(x_i)|}, \tag{2.26}$$

where the x_i are the roots of the function f. Per constructionem, the function $\omega(k)-\omega_\mathrm{q}$ has only one real root at $k=k_\mathrm{q}$. Subsequently, we have

$$\delta(\omega(k)-\omega_\mathrm{q}) = \delta(k-k_\mathrm{q})/c. \tag{2.27}$$

With this, the equation of motion becomes

$$\begin{aligned}\dot{\tilde{c}}_e(t) &= -g_0^2\tilde{c}_e(t)\int_0^\infty \mathrm{d}k\,\pi\delta(\omega(k)-\omega_\mathrm{q}) \\ &= -\frac{\pi g_0^2}{c}\tilde{c}_e(t)\int_0^\infty \mathrm{d}k\,\delta(k-k_\mathrm{q}) \\ &= -\frac{\pi g_0^2}{c}\tilde{c}_e(t) \\ &= -\frac{\Gamma}{2}\tilde{c}_e(t),\end{aligned}$$

where we have introduced the *qubit decay rate* $\Gamma \equiv 2\pi g_0^2/c$. The amplitude for the qubit excitation in rotating frame is then given by

$$\tilde{c}_e(t) = e^{-\Gamma t/2}, \tag{2.28}$$

where we have inserted the initial condition $c_e(0)=1$ [see Eq. (2.3)]. By transforming back to the amplitude $c_e(t)$, we obtain

$$c_e(t) = \tilde{c}_e(t)e^{-i\omega_\mathrm{q}t} = e^{-(\Gamma/2+i\omega_\mathrm{q})t}. \tag{2.29}$$

Finally, we can compute the excitation probability

$$P_e(t) = |c_e(t)|^2 = e^{-\Gamma t}. \tag{2.30}$$

The excited state population of the qubit shows exponential decay to the ground state by spontaneous photon emission. The ability to reproduce this experimentally observed decay is one of the main results of Wigner-Weisskopf theory [32].

With $\tilde{c}_e(t)$, we can calculate the amplitude for the photonic mode excitation

$$\begin{aligned}\tilde{c}(k;t) &= -ig_0\,\theta(k)\int_0^t \mathrm{d}t'\,\tilde{c}_e(t')\,e^{-i[\omega_\mathrm{q}-\omega(k)]t'} \\ &= \frac{ig_0\,\theta(k)}{\Gamma/2-i\Delta}\left[e^{-(\Gamma/2-i\Delta)t}-1\right],\end{aligned} \tag{2.31}$$

where $\Delta \equiv \omega(k)-\omega_\mathrm{q}$ is the detuning of the field mode frequency from the qubit transition frequency. By transforming back to the amplitude $c(k;t)$, we obtain

$$\begin{aligned}c(k;t) &= \tilde{c}(k;t)e^{-i\omega(k)t} \\ &= \frac{ig_0\,\theta(k)}{\Gamma/2-i\Delta}\left[e^{-(\Gamma/2+i\omega_\mathrm{q})t}-e^{-i\omega(k)t}\right].\end{aligned} \tag{2.32}$$

2.2.2 Emission spectrum

The emission spectrum is given by [see Eq. (2.9)]

$$\begin{aligned} S(k;t) &= |c(k;t)|^2 \\ &= \frac{g_0^2\,\theta(k)}{(\Gamma/2)^2+\Delta^2}\left(1+e^{-\Gamma t}-e^{-\Gamma t/2}\left\{e^{i[\omega(k)-\omega_\mathrm{q}]t}+e^{-i[\omega(k)-\omega_\mathrm{q}]t}\right\}\right) \\ &= \frac{g_0^2\,\theta(k)}{(\Gamma/2)^2+\Delta^2}\left[1+e^{-\Gamma t}-2e^{-\Gamma t/2}\cos(\Delta t)\right]. \end{aligned} \tag{2.33}$$

2.2.3 Single-photon pulse

In general, the single-photon pulse is given by [see Eq. (2.14)]

$$\begin{aligned} n(x,t) &= \frac{1}{2\pi}\left|\int_{-\infty}^{+\infty}\mathrm{d}k\,e^{ikx}c(k;t)\right|^2 \\ &= \frac{g_0^2}{2\pi}\left|\int_0^{\infty}\frac{\mathrm{d}k}{\Gamma/2-i\Delta}\left[e^{-(\Gamma/2+i\omega_\mathrm{q})t}-e^{-i\omega(k)t}\right]e^{ikx}\right|^2. \end{aligned} \tag{2.34}$$

For this integrand, we cannot perform contour integration together with the residue theorem, except for the linear case, i.e. $\omega(k)=ck$[2]. For the latter, we can use that $\Gamma \ll \omega_\mathrm{q}$ in the Markov regime to write

$$\begin{aligned} n(x,t) &\approx \frac{g_0^2}{2\pi}\left|\int_{-\infty}^{+\infty}\frac{\mathrm{d}k}{\Gamma/2-i\Delta}\left[e^{-(\Gamma/2+i\omega_\mathrm{q})t}-e^{-ickt}\right]e^{ikx}\right|^2 \\ &\equiv \frac{g_0^2}{2\pi}\left|\int_{-\infty}^{+\infty}\mathrm{d}k\,f(k)\right|^2, \end{aligned} \tag{2.35}$$

where $\Delta = ck-\omega_\mathrm{q}$. Using the residue theorem, the integral of a function $f(z)$ over a closed contour C is given by [35]

$$\oint_C \mathrm{d}z\,f(z) = \pm 2\pi i\sum_n \operatorname*{Res}_{z=z_n}[f(z)], \tag{2.36}$$

where $\sum_n \operatorname*{Res}_{z=z_n}[f(z)]$ is the sum of the residues of $f(z)$ at its poles z_n within the contour C. The sign depends on the direction of integration. For contour integration in the complex plane, we first define the integrand by analytic continuation $k \to z \in \mathbb{C}$ as

$$\begin{aligned} f(z) &:= \frac{1}{\Gamma/2-i(cz-\omega_\mathrm{q})}\left[e^{-(\Gamma/2+i\omega_\mathrm{q})t}-e^{-iczt}\right]e^{izx} \\ &= \frac{1}{\Gamma/2-i(cz-\omega_\mathrm{q})}\left[e^{-(\Gamma/2+i\omega_\mathrm{q})t}e^{izx}-e^{-iz(ct-x)}\right]. \end{aligned} \tag{2.37}$$

[2] This is due to terms of higher order in k occurring in the exponential $e^{-i\omega(k)t}$.

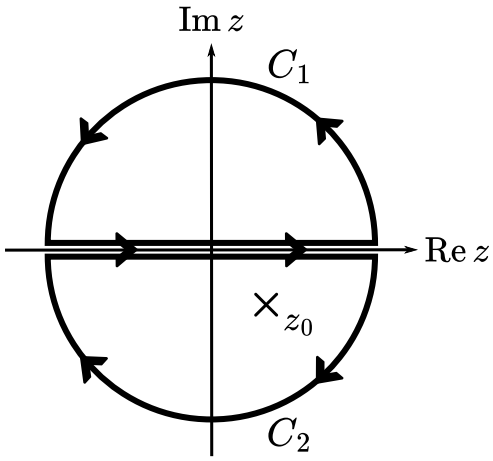

Figure 2.2: Integration contours for pulse calculation.

The integrand has a simple pole at $z_0 = (\omega_q - i\Gamma/2)/c$. For the integration, we have to distinguish between the cases $x < 0$, $x \geq 0$, $ct - x < 0$ and $ct - x \geq 0$. It is therefore convenient to write $f(z)$ as the sum of two functions

$$f(z) = f_1(z) + f_2(z), \quad \text{with} \quad f_1(z) \equiv \frac{e^{-(\Gamma/2+i\omega_q)t}e^{izx}}{\Gamma/2 - i(cz - \omega_q)}, \quad f_2(z) \equiv \frac{-e^{-iz(ct-x)}}{\Gamma/2 - i(cz - \omega_q)}. \tag{2.38}$$

For $x \geq 0$, the integral of f_1 vanishes, because we have to close the contour in the upper half-plane[3] (see contour C_1 in Fig. 2.2), but the pole z_0 is not enclosed by the contour. For f_2, we have two cases, $ct - x \geq 0$ and $ct - x < 0$ with $x \geq 0$. For $ct - x \geq 0$, we close the contour in the lower half-plane (see contour C_2 in Fig. 2.2), by which the pole is enclosed. For $ct - x < 0$, we have to close the contour in the upper half-plane (see contour C_1 in Fig. 2.2) and the integral again vanishes, because the pole is not enclosed. For $x < 0$, we have $ct - x = ct + |x| > 0$, which leads to a contribution to the integral from both f_1 and f_2.

By the residue theorem, the integral over the real k-axis is then given by

$$\int_{-\infty}^{+\infty} \mathrm{d}k\, f(k) = -2\pi i\, \theta(x)\theta(ct - x) \operatorname*{Res}_{z=z_0} [f_2(z)] - 2\pi i\, \theta(-x) \operatorname*{Res}_{z=z_0} [f(z)]\,, \tag{2.39}$$

where $\theta(\cdot)$ denotes the Heaviside function. The residue of a function $f(z)$ at its simple pole z_0 is given by [35]

$$\operatorname*{Res}_{z=z_0} [f(z)] = \lim_{z \to z_0} (z - z_0) f(z). \tag{2.40}$$

[3] We want to choose the integration contour, such that the integral over the half-circle vanishes asymptotically and we are left with the integral over the real axis.

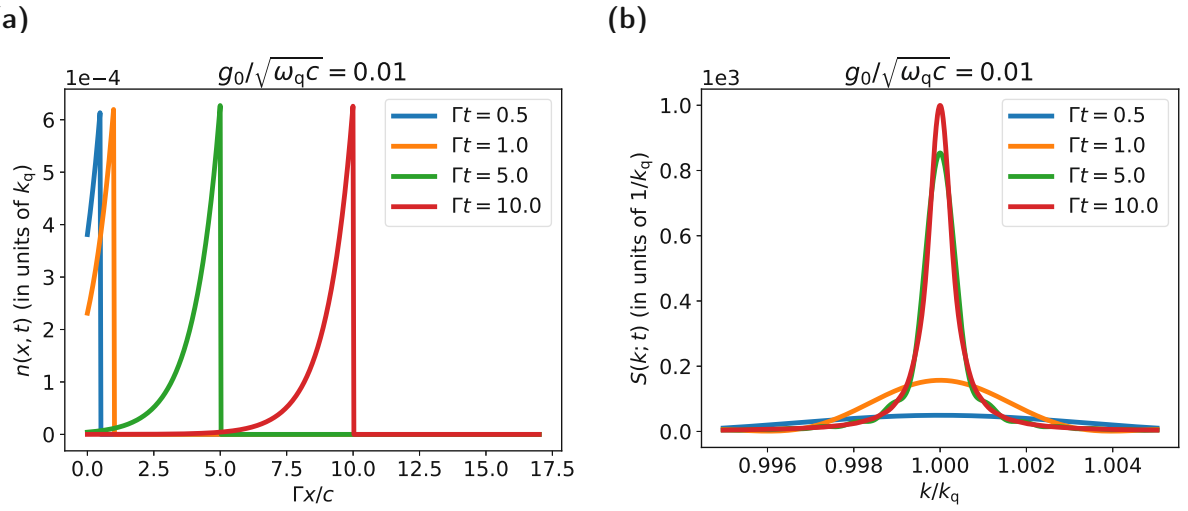

Figure 2.3: (a) Emitted pulses and (b) spectrum for a linear dispersion and for different times Γt.

Calculating the respective residues yields

$$\begin{aligned}
\operatorname*{Res}_{z=z_0}\left[f_2(z)\right] &= \lim_{z\to z_0}(z-z_0)f_2(z) \\
&= \lim_{z\to z_0} -\frac{i}{c}e^{-iz(ct-x)} \\
&= -\frac{i}{c}e^{-(\Gamma/2+i\omega_q)(ct-x)/c}, \\
\operatorname*{Res}_{z=z_0}\left[f(z)\right] &= \lim_{z\to z_0}(z-z_0)f(z) \\
&= \lim_{z\to z_0}\frac{i}{c}\left[e^{-(\Gamma/2+i\omega_q)t}e^{izx} - e^{-iz(ct-x)}\right] \\
&= 0.
\end{aligned} \tag{2.41}$$

The fact, that the residue of $f(z)$ at the pole z_0 vanishes is consistent with the general model, because the qubit only couples to positive modes, i.e. the pulse can only be emitted to the right ($x > 0$). Subsequently, Eq. (2.39) becomes

$$\int_{-\infty}^{+\infty}\mathrm{d}k\, f(k) = -\theta(x)\theta(ct-x)\frac{2\pi}{c}e^{-(\Gamma/2+i\omega_q)(ct-x)/c}. \tag{2.42}$$

Finally, we get an expression for the single-photon pulse [see Eq. (2.35)]

$$\begin{aligned}
n(x,t) &= \frac{g_0^2}{2\pi}\left|\int_{-\infty}^{+\infty}\mathrm{d}k\, f(k)\right|^2 \\
&= \theta(x)\theta(ct-x)\frac{2\pi g_0^2}{c^2}e^{-\Gamma(ct-x)/c} \\
&= \theta(x)\theta(ct-x)\frac{\Gamma}{c}e^{-\Gamma(ct-x)/c}.
\end{aligned} \tag{2.43}$$

In Fig. 2.3, we plot the single-photon pulse and the spectrum for different times t for a linear dispersion relation, i.e. $\omega(k) = ck$ and a coupling strength of $g_0/\sqrt{\omega_q c} = 0.01$.

Typical for spontaneous emission in the Wigner-Weisskopf regime [32], the pulse is asymmetrically stretched along the propagation direction, with a sharp front edge and a long exponential tail [see Fig. 2.3(a)].

In Fig. 2.3(b), we see that the emission spectrum builds up to a Lorentzian with FWHM[4] of Γ for increasing time. This makes sense, because for $t \to \infty$, it is a perfect Lorentzian, as we see mathematically from the form of $S(k;t)$ given by Eq. (2.33). Physically, according to Wigner-Weisskopf theory, after infinite time, the photon surely is emitted into the field and the qubit is in the ground state. The corresponding emission spectrum for a single photon emitted into free space is a perfect Lorentzian. It is also good to note, that because of the Heisenberg uncertainty relation, $\Delta E\, \Delta t \geq \hbar/2$, the energy uncertainty is big for small times t, which shows in the broad spectrum. For increasing times, the energy uncertainty gets smaller, which shows in the narrowing spectrum.

[4]FWHM = full width at half maximum

3 Single-Photon Transfer

In this chapter, we study two qubits chirally coupled to a 1D waveguide in order to understand the single-photon absorption behaviour of the second qubit. In particular, we calculate an analytic expression for the excitation probability of the second qubit for a linear dispersion in the chiral waveguide. We subsequently discuss the problems arising with such a linear dispersion. In order to overcome these problems, we extend our analysis to non-linear dispersion relations, which are engineered towards an improved single-photon absorption by the second qubit. Finally, we address the verification of the results obtained with non-linear dispersion relations using exact diagonalization.

3.1 Single-photon absorption in a two-qubit system

We consider the situation, where two identical qubits are coupled to a 1D photonic waveguide (see Fig. 3.1). Initially, the first (left) qubit is in the excited state, while the second (right) qubit is in the ground state. For this two-qubit system, we want to calculate the excitation probability of the second qubit in order to understand the absorption of an emitted single-photon pulse by a second qubit. The calculations are carried out in the Wigner-Weisskopf formalism, which was presented in Sec. 2.1.

3.1.1 Dynamics of the two-qubit system

The EOMs [see Eqs. (2.7)-(2.8)] for two qubits read

$$\dot{c}_{1,2}(t) = -i\omega_{\mathrm{q}} c_{1,2}(t) - i\int_0^\infty \mathrm{d}k\, g_{1,2}(k) c(k;t), \tag{3.1}$$

$$\dot{c}(k;t) = -i\omega(k) c(k;t) - i\left[g_1^*(k)c_1(t) + g_2^*(k)c_2(t)\right]. \tag{3.2}$$

As a first step, we again define slowly varying amplitudes

$$\tilde{c}_{1,2}(t) := c_{1,2}(t)e^{i\omega_{\mathrm{q}}t}, \quad \tilde{c}(k;t) := c(k;t)e^{i\omega(k)t}, \tag{3.3}$$

for which Eqs. (3.1)-(3.2) take the form

$$\dot{\tilde{c}}_1(t) = -i\int_0^\infty \mathrm{d}k\, g_1(k)\tilde{c}(k;t)e^{-i[\omega(k)-\omega_{\mathrm{q}}]t}, \tag{3.4}$$

$$\dot{\tilde{c}}_2(t) = -i\int_0^\infty \mathrm{d}k\, g_2(k)\tilde{c}(k;t)e^{-i[\omega(k)-\omega_{\mathrm{q}}]t}, \tag{3.5}$$

$$\dot{\tilde{c}}(k;t) = -i\left[g_1^*(k)\tilde{c}_1(t) + g_2^*(k)\tilde{c}_2(t)\right]e^{-i[\omega_{\mathrm{q}}-\omega(k)]t}. \tag{3.6}$$

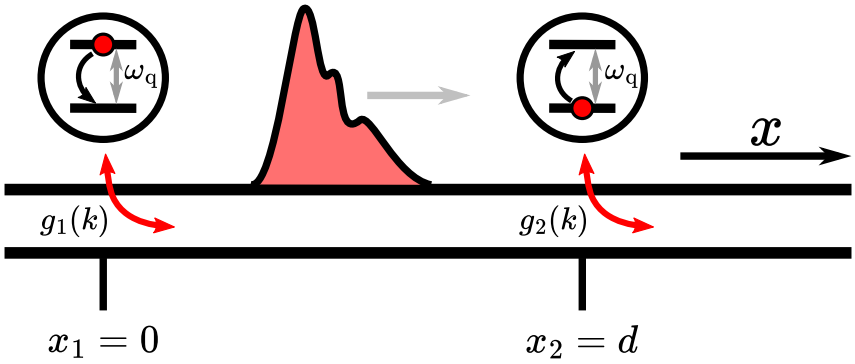

Figure 3.1: Two qubits chirally coupled to a 1D photonic waveguide.

For the calculations, we assume spectrally flat couplings around the qubit transition frequency,

$$g_1(k) = g_0\,\theta(k), \tag{3.7}$$
$$g_2(k) = g_0\,\theta(k)e^{ikd}, \tag{3.8}$$

where e^{ikd} is the pulse propagation phase. We impose the initial conditions stated in Eq. (2.3). By formal integration of Eq. (3.6), we obtain

$$\begin{aligned}
\tilde{c}(k;t) &= -i\int_0^t \mathrm{d}t'\ \left[g_1^*(k)\tilde{c}_1(t') + g_2^*(k)\tilde{c}_2(t')\right] e^{i\Delta t'} \\
&= -i\int_0^t \mathrm{d}t'\, g_1^*(k)\ \underbrace{\tilde{c}_1(t')}_{=e^{-\Gamma t'/2}}\ e^{i\Delta t'} - i\int_0^t \mathrm{d}t'\, g_2^*(k)\ \underbrace{\tilde{c}_2(t')}_{\to \tilde{c}_2(t)}\ e^{i\Delta t'} \\
&\simeq -i\int_0^t \mathrm{d}t'\, g_1^*(k)e^{-(\Gamma/2-i\Delta)t'} - i\tilde{c}_2(t)\int_0^t \mathrm{d}t'\, g_2^*(k)e^{i\Delta t'} \\
&\simeq -ig_0\int_0^t \mathrm{d}t'\, e^{-(\Gamma/2-i\Delta)t'} - i\pi g_0 e^{-ikd}\ \underbrace{\delta(\Delta)}_{=\delta(k-k_q)/c}\ \tilde{c}_2(t) \\
&= ig_0\frac{e^{-(\Gamma/2-i\Delta)t}-1}{\Gamma/2-i\Delta} - i\frac{\pi g_0}{c}e^{-ikd}\delta(k-k_q)\tilde{c}_2(t),
\end{aligned}$$

where $\Delta = \omega(k) - \omega_q$. In this calculation, we have used the result for the single-qubit emission (see Sec. 2.2.1) to set $\tilde{c}_1(t) = e^{-\Gamma t/2}$. This is justified because the chirality of the waveguide decouples the dynamics of the first qubit from the second qubit. Now, we can plug the expression for $\tilde{c}(k;t)$ into Eq. (3.5), which yields

$$\begin{aligned}
\dot{\tilde{c}}_2(t) &= -i\int_0^\infty \mathrm{d}k\, g_2(k)\tilde{c}(k;t)e^{-i\Delta t} \\
&= g_0^2\int_0^\infty \mathrm{d}k\, e^{ikd}\,\frac{e^{-(\Gamma/2-i\Delta)t}-1}{\Gamma/2-i\Delta}\,e^{-i\Delta t} - \frac{\pi g_0^2}{c}\tilde{c}_2(t)\int_0^\infty \mathrm{d}k\,\delta(k-k_q) \\
&= g_0^2\int_0^\infty \mathrm{d}k\,\frac{e^{ikd}\left(e^{-\Gamma t/2}-e^{-i\Delta t}\right)}{\Gamma/2-i\Delta} - \frac{\Gamma}{2}\tilde{c}_2(t), \quad \text{with} \quad \Gamma = \frac{2\pi g_0^2}{c}.
\end{aligned}$$

The inhomogeneous differential equation for the amplitude $\tilde{c}_2$ has the form

$$\dot{\tilde{c}}_2(t) = f(t) - \frac{\Gamma}{2}\tilde{c}_2(t). \tag{3.9}$$

By variation of parameters [35], the general solution to Eq. (3.9) is given by

$$\tilde{c}_2(t) = \alpha(t)e^{-\Gamma t/2}, \quad \text{if} \quad \dot{\alpha}(t) = f(t)e^{\Gamma t/2}. \tag{3.10}$$

Through simple formal integration, we obtain

$$\begin{aligned}
\alpha(t) &= \underbrace{\alpha(0)}_{=0} + \int_0^t \mathrm{d}t'\, f(t')e^{\Gamma t'/2} \\
&= g_0^2 \int_0^t \mathrm{d}t' \int_0^\infty \mathrm{d}k\, \frac{e^{ikd}\left(e^{-\Gamma t'/2} - e^{-i\Delta t'}\right)}{\Gamma/2 - i\Delta} e^{\Gamma t'/2} \\
&= g_0^2 \int_0^t \mathrm{d}t' \int_0^\infty \mathrm{d}k\, \frac{e^{ikd}\left[1 - e^{(\Gamma/2 - i\Delta)t'}\right]}{\Gamma/2 - i\Delta} \\
&= \underbrace{g_0^2 \int_0^\infty \mathrm{d}k\, \frac{te^{ikd}}{\Gamma/2 - i\Delta}}_{\approx 0} - g_0^2 \int_0^\infty \mathrm{d}k\, \frac{e^{ikd}}{\Gamma/2 - i\Delta} \int_0^t \mathrm{d}t'\, e^{(\Gamma/2 - i\Delta)t'}.
\end{aligned}$$

For a linear dispersion, the first term is zero, because the pole of the integrand lies in the lower half-plane but for contour integration, we would have to close the contour in the upper half-plane (note that $d > 0$). Also, for a non-linear dispersion [see Eq. (2.23)], we numerically find that the first term is very small, so it can be neglected. We are left with

$$\begin{aligned}
\alpha(t) &= -g_0^2 \int_0^\infty \mathrm{d}k\, \frac{e^{ikd}}{\Gamma/2 - i\Delta} \int_0^t \mathrm{d}t'\, e^{(\Gamma/2 - i\Delta)t'} \\
&= -g_0^2 \int_0^\infty \mathrm{d}k\, \frac{e^{ikd}\left[e^{(\Gamma/2 - i\Delta)t} - 1\right]}{(\Gamma/2 - i\Delta)^2}.
\end{aligned} \tag{3.11}$$

The general solution for the amplitude $\tilde{c}_2$ is then given by

$$\tilde{c}_2(t) = \alpha(t)e^{-\Gamma t/2} = -g_0^2 \int_0^\infty \mathrm{d}k\, \frac{e^{ikd}\left(e^{-i\Delta t} - e^{-\Gamma t/2}\right)}{(\Gamma/2 - i\Delta)^2}. \tag{3.12}$$

The excitation probability is calculated by

$$P_2(t) = |\tilde{c}_2(t)|^2. \tag{3.13}$$

3.1.2 Maximum absorption for a linear dispersion

Now we want to find an analytic expression for the excitation probability of the second qubit for a waveguide with linear dispersion. This is essential in order to obtain a fundamental

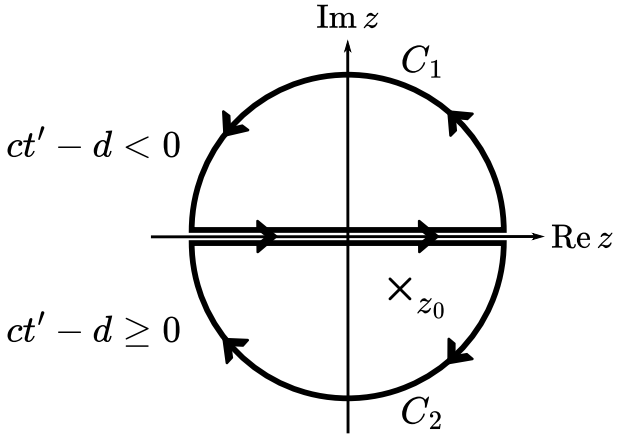

Figure 3.2: Integration contours for the calculation of the excitation probability of the second qubit.

limit for the single-photon absorption in this regime. We start again with the expression for $\alpha(t)$ given in Eq. (3.11), but calculate the k-integral first, i.e.

$$\begin{aligned}\alpha(t) &= -g_0^2 \int_0^\infty \mathrm{d}k \, \frac{e^{ikd}}{\Gamma/2 - i\Delta} \int_0^t \mathrm{d}t' \, e^{(\Gamma/2 - i\Delta)t'} \\ &= -g_0^2 \int_0^t \mathrm{d}t' \, e^{(\Gamma/2 + i\omega_\mathrm{q})t'} \int_0^\infty \mathrm{d}k \, \frac{e^{-ik(ct'-d)}}{\Gamma/2 - i\Delta},\end{aligned} \tag{3.14}$$

where $\Delta = ck - \omega_\mathrm{q}$. The k-integral can be calculated by contour integration together with the residue theorem in the complex plane (see also the pulse calculation in Sec. 2.2.3). In the Markov regime, the FWHM of the Lorentzian $\Gamma \ll \omega_\mathrm{q}$. With this, we can write

$$\int_0^\infty \mathrm{d}k \, \frac{e^{-ik(ct'-d)}}{\Gamma/2 - i\Delta} \approx \int_{-\infty}^{+\infty} \mathrm{d}k \, \frac{e^{-ik(ct'-d)}}{\Gamma/2 - i\Delta}. \tag{3.15}$$

We define the integrand by analytic continuation $k \to z \in \mathbb{C}$ as

$$f(z) := \frac{e^{-iz(ct'-d)}}{\Gamma/2 - i(cz - \omega_\mathrm{q})}. \tag{3.16}$$

The integrand $f(z)$ has a simple pole at $z_0 = (\omega_\mathrm{q} - i\Gamma/2)/c$. For contour integration, we have to distinguish between the cases $ct' - d < 0$ and $ct' - d \geq 0$. For $ct' - d < 0$, the integral of $f(z)$ vanishes, because we have to close the contour in the upper half-plane (see contour C_1 in Fig. 3.2), but the pole z_0 is not enclosed by the contour. For the latter case, we close the contour in the lower half-plane (see contour C_2 in Fig. 3.2), by which the pole is enclosed.

By the residue theorem, the integral over the real k-axis is then given by

$$\int_{-\infty}^{+\infty} \mathrm{d}k \, \frac{e^{-ik(ct'-d)}}{\Gamma/2 - i\Delta} = -2\pi i \, \theta(ct' - d) \operatorname*{Res}_{z=z_0} [f(z)] \,. \tag{3.17}$$

Calculating the residue yields

$$\begin{aligned}\operatorname*{Res}_{z=z_0}[f(z)] &= \lim_{z\to z_0}(z-z_0)f(z)\\ &= \frac{i}{c}e^{-(ct'-d)(\Gamma/2+i\omega_q)/c}.\end{aligned}$$

Subsequently, Eq. (3.17) becomes

$$\begin{aligned}\int_{-\infty}^{+\infty}\mathrm{d}k\,\frac{e^{-ik(ct'-d)}}{\Gamma/2-i\Delta} &= -2\pi i\,\theta(ct'-d)\operatorname*{Res}_{z=z_0}[f(z)]\\ &= \theta(ct'-d)\frac{2\pi}{c}e^{-(ct'-d)(\Gamma/2+i\omega_q)/c}.\end{aligned}$$

By inserting the expression for the k-integral into Eq. (3.14), we obtain

$$\begin{aligned}\alpha(t) &= -g_0^2\int_0^t \mathrm{d}t'\,e^{(\Gamma/2+i\omega_q)t'}\int_0^\infty \mathrm{d}k\,\frac{e^{-ik(ct'-d)}}{\Gamma/2-i\Delta}\\ &= -\frac{2\pi g_0^2}{c}e^{(\Gamma/2+i\omega_q)d/c}\int_0^t \mathrm{d}t'\,\theta(ct'-d)\\ &= -\frac{\Gamma}{c}(ct-d)e^{(\Gamma/2+i\omega_q)d/c}.\end{aligned}$$

The amplitude $\tilde{c}_2$ is then given by

$$\begin{aligned}\tilde{c}_2(t) &= \alpha(t)e^{-\Gamma t/2}\\ &= -\frac{\Gamma}{c}(ct-d)e^{-\Gamma(ct-d)/(2c)}e^{i\omega_q d/c}.\end{aligned}$$

Finally, we obtain the excitation probability of the second qubit

$$P_2(t) = |\tilde{c}_2(t)|^2 = \frac{\Gamma^2}{c^2}(ct-d)^2e^{-\Gamma(ct-d)/c}. \tag{3.18}$$

In Fig. 3.3, we plot the excitation probability of the second qubit as a function of time. For this plot, we chose a qubit separation of $\Gamma d/c = 500$ and a coupling strength of $g_0/\sqrt{\omega_q c} = 0.01$. We also want to know the maximum of $P_2(t)$, because it corresponds to the maximum absorption of a freely propagating pulse by a second qubit in a 1D chiral waveguide with a linear dispersion relation. The maximum of $P_2(t)$ can be analytically calculated to be

$$\max P_2^{\mathrm{lin}}(t) = 4/e^2 \approx 0.54 \tag{3.19}$$

at time $t_{\max} = (2c+\Gamma d)/(\Gamma c)$.

This means, that we have a maximum absorption of only about 54% in a 1D chiral waveguide with a linear dispersion relation [22].

With this, we have derived a fundamental limit for the single-photon absorption for a linear dispersion relation. Subsequently, in order to achieve an enhanced single-photon absorption, we will use a non-linear dispersion relation to explore different regions of curvature of the band. In the following, we present the non-linear dispersion relation and explain its construction.

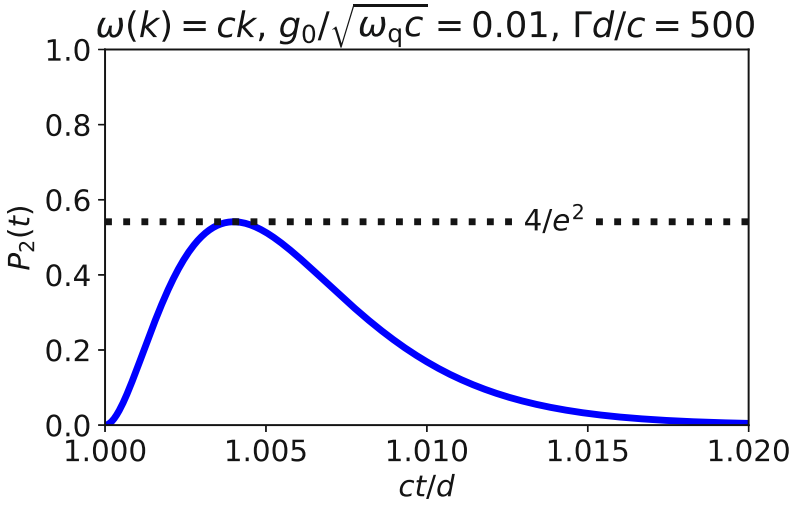

Figure 3.3: Excitation probability of the second qubit as a function of time for a linear dispersion relation.

3.2 Non-linear dispersion relation

As we have seen in the previous section, a linear dispersion greatly limits the single-photon absorption. Subsequently, for the chiral waveguide, we consider an arbitrary dispersion relation characterised by a polynomial functional form

$$\begin{aligned} \omega(k) - \omega_q &= \omega_q \xi \prod_{n=1}^{N/2} \frac{(\xi - z_n)(\xi - z_n^*)}{|z_n|^2} \\ &= \omega_q \sum_{n=1}^{N} a_n \xi^n, \quad \text{with} \quad \xi \equiv \frac{k - k_q}{k_q}, \end{aligned} \tag{3.20}$$

where the $z_n = z_{n,r} + i z_{n,i}$ are the complex roots of the detuning $\omega(k) - \omega_q$, N is the degree of the polynomial and the a_n are the polynomial coefficients. This form is in principle an expansion around $k = k_q$, such that the dispersion is linear in a region near the qubit. We restrict ourselves to only odd degrees N and choose the complex roots z_n, such that we surely have only one real root of the detuning at $k = k_q$ while all other $N - 1$ roots have a non-vanishing imaginary part. This ensures, that we have only one emission channel for the qubit. Multiple emission channels would correspond to having an effective multi-band waveguide, but we want to explore single-band physics. A dispersion relation shape, that would correspond to having a multi-band waveguide is shown in Fig. 3.4(a). Additionally, we choose the complex roots, z_n, such that local extrema of the dispersion relation, $\omega(k)$, do not come too close to the qubit transition frequency ω_q[1]. That way, we ensure that we operate in the Markov regime. Because local extrema of the band correspond to a

[1]For the explicit constraints on the complex roots, see Sec. 3.4.2.

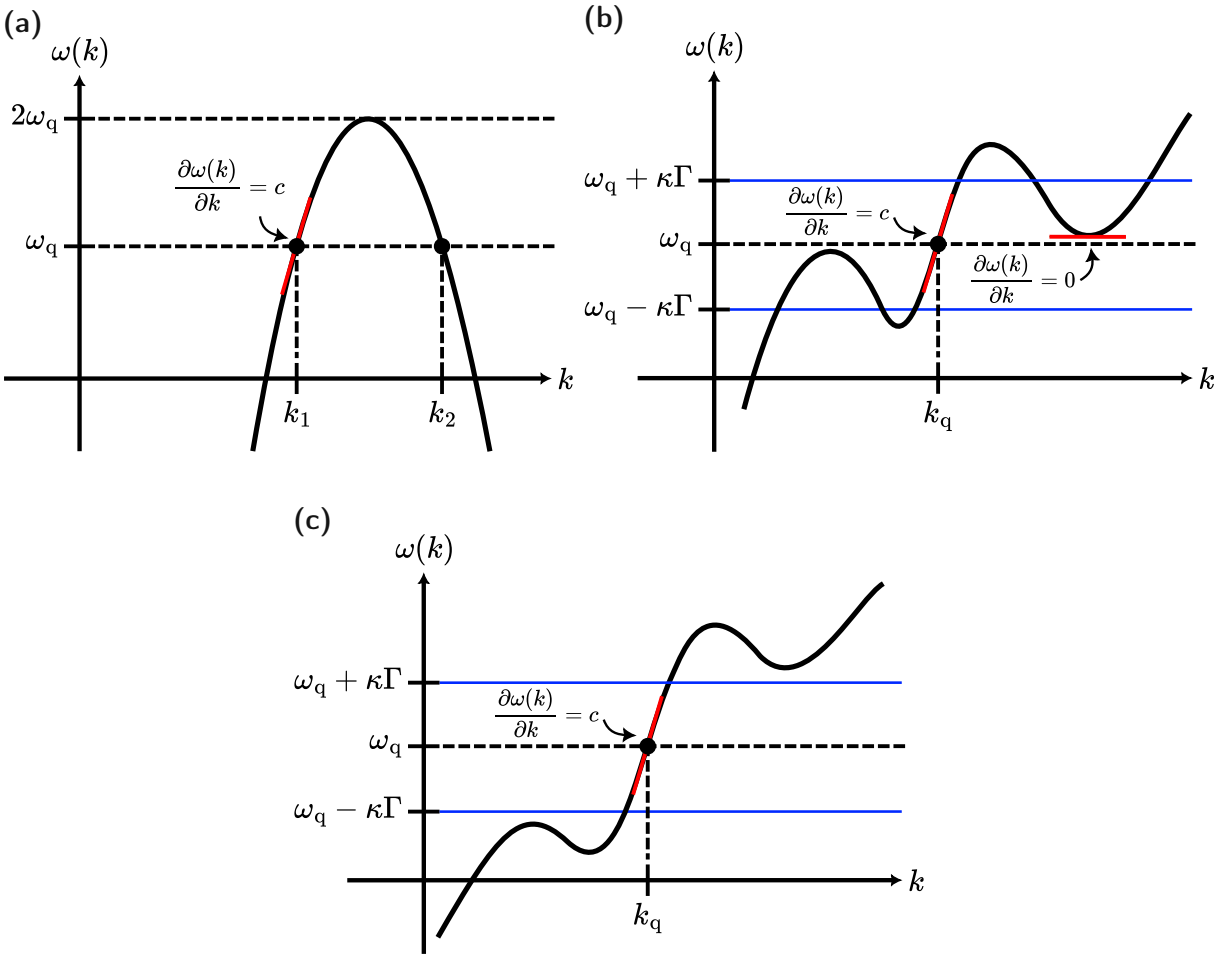

Figure 3.4: Construction of the non-linear dispersion relation. (a) A single band having a parabolic form with a maximum far away from the qubit frequency at $2\omega_q$, decreasing towards $k = \pm\infty$. This band cuts the qubit transition frequency ω_q at two modes k_1, k_2 with slope $|\partial\omega(k)/\partial k| = c$. In this regime, the Markov approximation is valid, but we have an effective two-band waveguide. (b) A single band which intersects the qubit transition frequency at $k = k_q$. Local extrema of the band, where $\partial\omega(k)/\partial k = 0$, are close to the qubit frequency, i.e. lie within a region of $2\kappa\Gamma$ around ω_q, where $\kappa \in \mathbb{N}$. Here, the Markov approximation fails, because we are effectively in a very strong coupling regime. (c) The desired shape, where a single band intersects the qubit transition frequency at $k = k_q$ and local extrema of the band are far away from the qubit transition frequency. We have one emission channel and operate in the Markov regime.

very small group velocity, the coupling near such extrema is effectively very strong, which contradicts the assumption of weak coupling for the Markov approximation. A dispersion relation shape that would violate the Markov approximation is shown in Fig. 3.4(b). An example for the desired dispersion relation is shown in Fig. 3.4(c). The construction allows to explore different curvatures of the band by choosing the polynomial degree N, i.e. the number of complex roots, and the roots themselves.

The derivative of the detuning with respect to k is given by

$$\partial_k \left[\omega(k) - \omega_\mathrm{q}\right] = c \sum_{n=1}^{N} n\, a_n \xi^{n-1}, \quad \text{with} \quad \xi \equiv \frac{k - k_\mathrm{q}}{k_\mathrm{q}}, \tag{3.21}$$

where we used $\omega_\mathrm{q} = c k_\mathrm{q}$. Evaluating the derivative at $k = k_\mathrm{q}$, which is per constructionem the only real root of the detuning, yields

$$\partial_k \left[\omega(k) - \omega_\mathrm{q}\right] \big|_{k=k_\mathrm{q}} = c, \tag{3.22}$$

because all terms in ξ^α, $\alpha \geq 1$ vanish. With this, we have verified, that the dispersion relation is indeed linear with a maximum slope of c near the qubit. For all dispersion relations constructed via Eq. (3.20), we thus have the same emission channel and the same decay rate, which is calculated with Wigner-Weisskopf theory (see Sec. 2.1).

3.3 Single-photon transfer optimization scheme

In the following, we present our approach to optimize the single-photon transfer, i.e. the absorption of a single photon by a second qubit, by engineering non-linear dispersion relations of the form discussed in Sec. 3.2. The optimization process is schematically depicted in Fig. 3.5.

This approach is solely based on the single-qubit description presented in Sec. 2.2. The basic idea behind this method is to use the time-reversal symmetry of the Schrödinger equation together with the chiral couplings, which allows for separate treatment of the emission and absorption processes. From time-reversal symmetry, we know that the time-reversed single-photon pulse can be perfectly absorbed by a single qubit. With this, in our chiral system, we obtain a "target pulse", which can be perfectly absorbed by the second qubit. This target pulse can then be used to perform numerical optimization, where the goal is to maximize the spatial overlap between the emitted single-photon pulse and the target pulse. The underlying theoretical ideas, calculations and the numerical optimization scheme are presented in detail in the following sections.

3.3.1 Time-reversal symmetry of the equations of motion

We remind ourselves of the EOMs describing a single qubit chirally coupled to a 1D waveguide. The EOMs in rotating frame read [see Eqs. (2.18)-(2.19)]

$$\dot{\tilde{c}}_e(t) = -i \int_0^\infty \mathrm{d}k\, g(k)\tilde{c}(k;t)e^{-i[\omega(k)-\omega_\mathrm{q}]t}, \tag{3.23}$$

$$\dot{\tilde{c}}(k;t) = -ig(k)\tilde{c}_e(t)e^{-i[\omega_\mathrm{q}-\omega(k)]t}, \tag{3.24}$$

where we assume, that $g(k) \in \mathbb{R}$. Now, we reverse the time ($t \to -t$) and take the complex conjugate of Eqs. (3.23)–(3.24), which yields

$$\dot{\tilde{c}}^*_e(-t) = -i \int_0^\infty \mathrm{d}k\, g(k)c^*(k;-t)e^{-i[\omega(k)-\omega_\mathrm{q}]t}, \tag{3.25}$$

$$\dot{\tilde{c}}^*(k;-t) = -ig(k)\tilde{c}^*_e(-t)e^{-i[\omega_\mathrm{q}-\omega(k)]t}. \tag{3.26}$$

We see, that the amplitudes $\tilde{c}^*_e(-t)$ and $\tilde{c}^*(k;-t)$ follow the same EOMs as the amplitudes $\tilde{c}_e(t)$ and $\tilde{c}(k;t)$. This means, that the pulse formed by the complex conjugated amplitudes $c^*(k;t_F)$, i.e. the time-reversed pulse, can be perfectly absorbed after the time t_F, which is precisely the duration of spontaneous emission of the initial pulse. From this, it becomes clear that perfect absorption is only possible for infinite time. Subsequently, we can set $\{c^*_e(t_F), c^*(k;t_F)\}$ as initial configuration for the amplitudes at $t = 0$, where $c^*_e(t_F) \simeq 0$. For calculation purposes, we choose a finite time t_F, where the pulse is (almost) fully emitted by the qubit, i.e. the qubit has (almost) fully decayed. For all numerical and analytical calculations in this thesis, we choose $\Gamma t_F = 10$, such that the excitation probability of the emitting qubit has decayed to $P_e(t_F) = e^{-10}$.

3.3.2 Pulse shifting in momentum space

From the time-reversal symmetry analysis in the previous section (Sec. 3.3.1), we know, that the perfectly absorbable single-photon pulse for the first qubit in our system is given in momentum space by

$$\zeta^0_k := c^*(k;t_F). \tag{3.27}$$

This pulse corresponds to the pulse, which is emitted until the time t_F, but exactly mirrored at the first qubit (i.e. at $x = 0$) in position space. This means, that the pulse lies on the negative $x-$axis and can be perfectly absorbed by the first qubit after the time t_F. This time-reversal of the pulse is schematically depicted in Fig. 3.5(a).

Because we want the second qubit at position $x = d$ to perfectly absorb the emitted pulse, we have to shift the time-reversed pulse accordingly. In position space, we have

$$\zeta^0_x = \int \mathrm{d}k\, \zeta^0_k e^{ikx}. \tag{3.28}$$

By shifting the pulse in position space by the distance d towards the second qubit, we obtain

$$\zeta^d_x = \int \mathrm{d}k\, \zeta^0_k e^{ik(x-d)}. \tag{3.29}$$

The pulse shift towards the second qubit in position space is shown in Fig. 3.5(b). In momentum space, this shift corresponds to

$$\begin{aligned}\zeta_k^d &= \frac{1}{2\pi}\int \mathrm{d}x\, \zeta_x^d e^{-ikx} \\ &= e^{-ikd}\zeta_k^0 \\ &= e^{-ikd}c^*(k;t_F).\end{aligned} \tag{3.30}$$

With this, we have obtained the target pulse for the second qubit in momentum space.

3.3.3 Describing the pulse overlap by a cost function

Now that we know the target single-photon pulse for perfect excitation of the second qubit, we can let the emitted pulse from the first qubit evolve, which is trivial in momentum space,

$$e^{-i\omega(k)t}c(k;0) = e^{-i\omega(k)(t-t_F)}c(k;t_F). \tag{3.31}$$

The propagating pulse then has to perfectly overlap with the target pulse given by Eq. (3.30) at some point in time t in order for the pulse to be perfectly absorbed by the second qubit [see Fig. 3.5(c)]. With this, we can write down the optimization rule

$$\min_{a_n}\left\{\min_{t}\left[||e^{-i\omega(k)(t-t_F)}c(k;t_F) - e^{-ikd}c^*(k;t_F)||_2\right]\right\}, \tag{3.32}$$

with $||f(k)||_2 = \int \mathrm{d}k\, |f(k)|^2$.

From the optimization rule given by Eq. (3.32), we can define the cost function,

$$\tilde{\mathcal{F}}(t) := ||e^{-i\omega(k)(t-t_F)}c(k;t_F) - e^{-ikd}c^*(k;t_F)||_2, \tag{3.33}$$

which corresponds to the overlap between the target pulse and the propagating pulse in the waveguide. The cost function in Eq. (3.33) is oscillating with frequency $\omega \approx \omega_\mathrm{q}$. This global phase does not affect the absorption of the pulse by the second qubit. In order to get rid of the global phase, we can write the cost function in the form

$$\mathcal{F}(t) := 2\left(1 - \left|\int_0^\infty \mathrm{d}k\, c_1^*(k;t)c_2(k)\right|\right). \tag{3.34}$$

In the following, we will always use this form of the cost function, and refer to it as "cost function". If the pulse overlap is perfect, the cost function reaches its minimum, i.e. $\mathcal{F}(t) = 0$, and the second qubit is perfectly excited. The minimization of the cost function is performed over the evolution time, t, and over the polynomial coefficients in the dispersion relation, a_n. Because the goal of the optimization in this approach is to maximize the pulse overlap, we will refer to this method as "pulse overlap method".

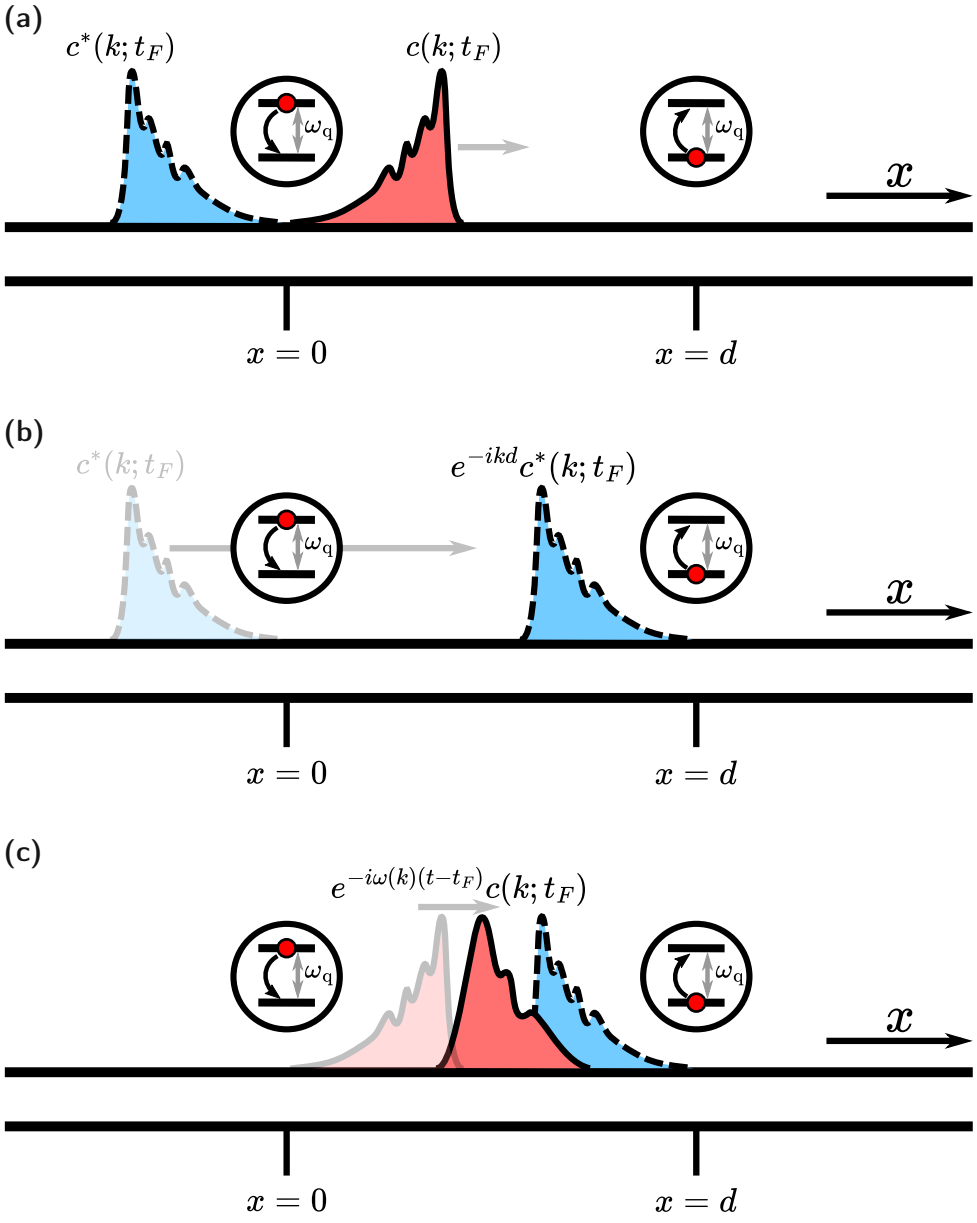

Figure 3.5: Pulse overlap scheme in position space. (a) The single-photon pulse (red) is emitted by the qubit until the time $t = t_F$. The pulse is then time-reversed, i.e. mirrored at the qubit at $x = 0$ (blue). (b) The time-reversed pulse is shifted by the distance d towards the second qubit. The shifted pulse is the target pulse, which can be perfectly absorbed by the second qubit exactly after the time t_F. (c) The freely propagating pulse (red) is reshaped according to the non-linear dispersion relation and overlapped with the target pulse (blue). Through numerical optimization, the dispersion relation is engineered, such that the spatial overlap between the two pulses is maximized.

3.3.4 Verification of the optimization scheme

We now want to verify, that the cost function [see Eq. (3.34)] in our pulse overlap method corresponds to the excitation probability of the second qubit, which was calculated in Sec. 3.1 [see Eq. (3.12)]. This is important, because we have to confirm that we are really optimizing for the excitation of the second qubit. We look at the pulse overlap integral in the cost function [see Eq. (3.34)] in rotating frame,

$$\mathcal{F}_k(t) := \int_0^\infty \mathrm{d}k\, \tilde{c}_1^*(k;t)\tilde{c}_2(k), \tag{3.35}$$

where

$$\tilde{c}_1(k;t) \equiv e^{-i\omega(k)(t-t_F)}\tilde{c}(k;t_F), \quad \tilde{c}_2(k;t) \equiv e^{-ikd}\tilde{c}^*(k;t_F).$$

The amplitudes $\tilde{c}^*(k;t)$ evaluated at time $t = t_F$, where we choose $t_F = 10\,\Gamma^{-1}$, are given by [see Eq. (2.31)]

$$\tilde{c}(k;t_F) = \frac{ig_0}{\Gamma/2 - i\Delta}\left[\underbrace{e^{-(\Gamma/2+i\omega_\mathrm{q})t_F}}_{\approx 0} e^{i\omega(k)t_F} - 1\right] \simeq -\frac{ig_0}{\Gamma/2 - i\Delta}.$$

With this, we have

$$\mathcal{F}_k(t) = -g_0^2 \int_0^\infty \mathrm{d}k\, \frac{e^{-ikd}e^{i\omega(k)(t-t_F)}}{(\Gamma/2 + i\Delta)^2}. \tag{3.36}$$

By comparing this expression to the one obtained for the excitation amplitude of the second qubit (see Sec. 3.1),

$$\tilde{c}_2(t) = -g_0^2 \int_0^\infty \mathrm{d}k\, \frac{e^{ikd}\left(e^{-i\Delta t} - e^{-\Gamma t/2}\right)}{(\Gamma/2 - i\Delta)^2}, \tag{3.37}$$

we find, that the pulse overlap method is indeed equivalent to the description in Sec. 3.1 for large times, i.e.

$$P_2(t) = |\tilde{c}_2(t)|^2 \overset{t\to\infty}{=} |\mathcal{F}_k(t)|^2. \tag{3.38}$$

Since we are only interested in times $t > t_F = 10\,\Gamma^{-1}$, where the single-photon pulse is almost fully emitted, we are optimizing for the excitation of the second qubit. We can directly convert the cost function to the excitation probability of the second qubit by using Eq. (3.34),

$$P_2(t) \overset{t\to\infty}{=} \left[1 - \frac{\mathcal{F}(t)}{2}\right]^2. \tag{3.39}$$

3.4 Numerical details of the optimization

In the following, we present the numerical details regarding the pulse overlap method. This includes the optimization time window, the constraints on the complex roots of the detuning and further details regarding the numerical implementation.

3.4.1 Time window for the optimization

In order to choose a time window for the numerical minimization of the cost function, i.e. an estimate of when the maximum pulse overlap will occur, we take the group velocity at the qubit transition frequency,

$$\left.\frac{\partial\omega(k)}{\partial k}\right|_{k=k_\mathrm{q}} = c,$$

and calculate the time, where the pulse peak is at position $x_d = d - x_F$, with the full pulse length $x_F = ct_F$,

$$t_d = \frac{x_d}{c}.$$

We know, that the minimum of the cost function has to lie at a time greater than t_d, because the overlap of the two pulses cannot be optimal for this time. By adding the full pulse emission time t_F, we can be sure to capture the global minimum of the cost function, because after the time $t_d + t_F$, the pulse overlap cannot be maximal. Subsequently, we choose the following time interval for the optimization,

$$t \in [t_d, t_d + t_F], \tag{3.40}$$

which will be used for all numerical calculations.

3.4.2 Root constraints for the optimization

In order to make sure that we have only one emission channel for the qubit, i.e. that the detuning has only one real root at $k = k_\mathrm{q}$, and that we operate in the Markov regime, we construct the dispersion relation as given by Eq. (3.20) via the complex roots z_n of the detuning. Accordingly, we choose

$$\begin{aligned} &z_{n,r} \in (-\infty, \infty), \\ &|z_{n,i}| \in \begin{cases} [0,\infty), \text{ with } z_{n,r}^2 + z_{n,i}^2 > (6000\,\Gamma/\omega_\mathrm{q})^2, & \text{if } z_{n,r} < 0 \\ [6000\,\Gamma/\omega_\mathrm{q}, \infty), & \text{if } z_{n,r} \geq 0, \end{cases} \quad \forall n, \end{aligned} \tag{3.41}$$

which makes sure to discard a half-circular region centered at $z_{n,r} = 0$ with radius $R = 6000\,\Gamma/\omega_\mathrm{q}$ for all roots with negative real part, i.e. $z_{n,r} < 0$. For roots with a positive real part, i.e. $z_{n,r} \geq 0$, a strip of width $12000\,\Gamma/\omega_\mathrm{q}$ with the real axis as symmetry line is excluded. In Fig. 3.6, the root constraints are depicted in the complex plane, where the shaded area corresponds to the excluded region.

We set $6000\,\Gamma/\omega_\mathrm{q}$ as a lower limit, because the underlying Lorentzian decays slowly on the energy scale of Γ and we want only one emission channel, i.e. one single Lorentzian peak around $k = k_\mathrm{q}$ without any secondary peaks away from the resonance, also for higher polynomial degrees. The decay behaviour of the Lorentzian can be seen by looking at the form of the spectrum [see Eq. (2.33)],

$$S(x) \sim \frac{1}{\Gamma^2 + x^2}. \tag{3.42}$$

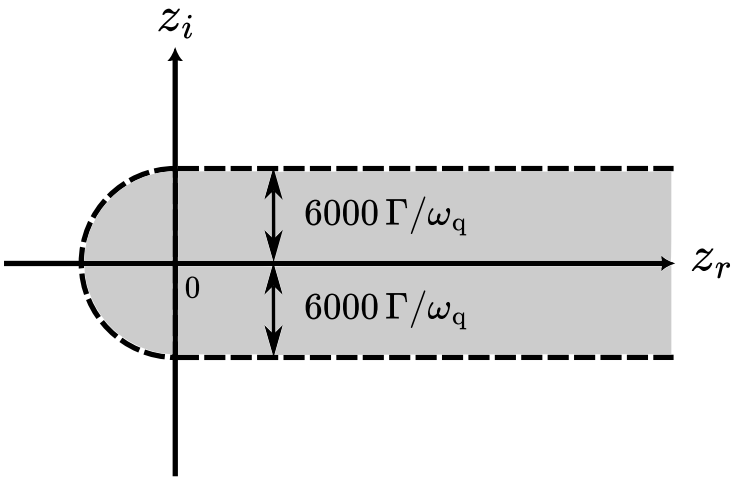

Figure 3.6: Root constraints in the complex plane. The grey area corresponds to the excluded region for the roots of the detuning $\omega(k) - \omega_q$.

We can approximate the decay of the Lorentzian by assuming that the decay rate Γ is negligible compared to x as

$$\frac{1}{\sqrt{\Gamma^2 + x^2}} \sim \frac{1}{x}. \tag{3.43}$$

If we choose, e.g. $x = 100$, the Lorentzian has decayed to 1% of its maximum height. We want a decay to at least 0.1% of the maximum height in order to obtain results in the Markov regime. Therefore a lower limit $\mathcal{O}(1000\,\Gamma/\omega_q)$ is sufficient.

3.4.3 Numerical implementation

Optimization process

The numerical process for optimizing the pulse overlap can be described as follows. For a fixed polynomial degree N and qubit separation d, we perform the following steps.

1. The initial values for the time t are Monte Carlo sampled. We sample n_S independent values. The samples are drawn from a uniform distribution over the interval $[t_d, t_d+t_F]$ (see Sec. 3.4.1).

2. The initial values for the complex roots of the detuning, z_n, are Monte Carlo sampled. We sample n_S independent parameter sets $\{z_{1,r}, \ldots, z_{n,r}; z_{1,i}, \ldots, z_{n,i}\}$, with n being the number of complex roots of the detuning. This means, for each set, we sample $2n$ values. The samples are drawn from a uniform distribution over the interval $[-10, 10]$ and $[6 \cdot 10^3\,\Gamma/\omega_q, 6 \cdot 10^4\,\Gamma/\omega_q]$ for the $z_{n,r}$ and $z_{n,i}$, respectively (see Sec. 3.4.2).

3. For each of the n_S sets of initial parameters $\{t; z_{1,r}, \ldots, z_{n,r}; z_{1,i}, \ldots, z_{n,i}\}$, a minimization of the cost function [see Eq. (3.34)] over the time t and the roots z_n is performed with the `Scipy` routine `scipy.optimize.minimize` [36, 37], which uses

a gradient descent optimizer algorithm. For the roots z_n, the constraints stated in Eq. (3.41) are used. The smallest minimum of the cost function achieved over all minimizations and the corresponding parameter set $\{t; z_{1,r}, \ldots, z_{n,r}; z_{1,i}, \ldots, z_{n,i}\}$ are then saved. The smallest minimum of the cost function will be referred to as "minimum of the cost function" for simplicity.

The number of Monte Carlo samples, n_S, is chosen, such that the optimizer converges to the global minimum of the cost function for the given qubit separation and not to some local minimum. This manifests as the smoothness of the graph when plotting the minima of the cost function obtained via the optimization over the qubit separation. (see Chap. 4).

Markov regime and numerical integration

In all calculations, we set $g_0/\sqrt{\omega_q c} = 0.01$, which makes sure that we operate in the Markov regime. In order to verify that we operate in this regime, we can check whether the probability is conserved. If we leave the Markov regime, this is not the case anymore due to additional emission channels or different physics. With the chosen coupling strength, the probability is conserved up to an absolute error of $\approx 0.2\%$ for all cases (see Appendix B).

For the involved numerical integrations over the k-axis, we use an integration stepsize of $\Delta k/k_q = 5 \cdot 10^{-6}$. The integration interval is bounded by

$$\begin{aligned} k_{\min} &= \max\left\{k_q\left(1 - \eta\Gamma/\omega_q\right), 0\right\}, \\ k_{\max} &= k_q\left(1 + \eta\Gamma/\omega_q\right), \end{aligned} \tag{3.44}$$

where $\eta \in \mathbb{N}$ and $k \in [k_{\min}, k_{\max}]$. This makes sure that the integration interval is adjusted according to the FWHM of the perfect Lorentzian at $t \to \infty$. Especially, we want to avoid any cutting of the tails by choosing a too narrow integration window[2]. For all numerical integrations, we therefore choose $\eta = 200$, because the underlying Lorentzians decay slowly on the energy scale of Γ.

3.5 Numerical verification of the optimization method

3.5.1 Exact diagonalization

In order to verify the results obtained with our pulse overlap method, we use exact diagonalization. Exact diagonalization (ED) is a numerical method to solve for the dynamics of a quantum system. In order to use ED, we have to discretize the equations of motion of the given system. The detailed discretization for the two-qubit system can be found in Appendix C. The discrete system dynamics can be expressed by the matrix equation

$$\partial_t \vec{c}\,(t) = -i\,\mathbf{M}\,\vec{c}\,(t), \tag{3.45}$$

[2]This is important for the probability conservation, see Appendix B.

where $\mathbf{M}$ is the hermitian matrix of the discrete two-qubit system, i.e. $\mathbf{M}^\dagger = \mathbf{M}$, and $\vec{c}(t) = [c_1(t), c_2(t), c_{k_1}(t), \ldots, c_{k_N}(t)]^T$ is the vector of the probability amplitudes of the qubit and mode excitation, respectively. The formal solution of Eq. (3.45) is given by

$$\vec{c}(t) = e^{-i\mathbf{M}t}\,\vec{c}(0). \tag{3.46}$$

Solving for the dynamics of the system then comes down to calculating the matrix exponential $e^{-i\mathbf{M}t}$. By inserting the unitary transformation matrix $\mathbf{S}$, with $\mathbf{S}\mathbf{S}^\dagger = \mathbb{1}$, Eq. (3.46) becomes

$$\vec{c}(t) = \mathbf{S}\, e^{-i\mathbf{D}t}\, \mathbf{S}^\dagger\, \vec{c}(0), \tag{3.47}$$

with $\mathbf{D} = \mathbf{S}^\dagger\, \mathbf{M}\, \mathbf{S}$. With this, the matrix exponentiation becomes trivial, because

$$e^{-i\mathbf{D}t} = \begin{pmatrix} e^{-i\lambda_1 t} & & & \\ & e^{-i\lambda_2 t} & & \\ & & \ddots & \\ & & & e^{-i\lambda_{N+2} t} \end{pmatrix}, \tag{3.48}$$

where the λ_i are the eigenvalues of the matrix $\mathbf{M}$. Thus, solving for the dynamics becomes numerically possible. The diagonalization of the matrix $\mathbf{M}$ is done numerically with an eigensolver[3]. The computational runtime of ED was tested be at least 10^2 times greater than the one of our pulse overlap method for the parameters that we were exploring. The minimization of the cost function using gradient descent is way more efficient than calculating the dynamics with ED. Thus, ED is not feasible for our purpose and we will only use it as verification method for our pulse overlap method.

3.5.2 Numerical validation for a linear dispersion relation

In order to validate the pulse overlap method, we apply it to a waveguide with linear dispersion. Here, we do not perform numerical optimization, but we know the analytical solutions for the single-photon pulse and the excitation probability of the second qubit. The results for the excitation probabilities of the two qubits are also compared to the solutions obtained via ED.

In Figs. 3.7(a) and 3.7(b), we plot the cost function and the pulse overlap in position space for a qubit separation of $\Gamma d/c = 20$, respectively. The pulse overlap is shown for the specific time t_{opt}, where the cost function is minimal. This time will be referred to as "optimal time". In Fig. 3.7(b), we also show the analytical solution for the pulse [see Eq. (2.43)] at the optimal time. In Fig. 3.7(c), we plot the dynamics of the excitation probability of the first qubit, calculated with ED and Wigner-Weisskopf theory [analytical solution, see Eq. (2.30)]. In Fig. 3.7(d), we compare the excitation probabilities of the second qubit calculated via the cost function and ED to the analytical solution given by Eq. (3.18) (see Sec. 3.1.2), respectively.

From the results, we find that the minimum of the cost function lies well within the chosen time window [see Fig. 3.7(a)]. The numerically calculated single-photon pulse

[3]We are using the `eigh` routine in `Python`, which operates on `LAPACK` routines.

matches very well with the analytical solution [see Fig. 3.7(b)], verifying that the numerical integration yields correct results. The plot also confirms, that the time-reversal and shifting of the pulse works properly. Fig. 3.7(c) shows that the results for the excitation probability of the first qubit calculated via the two methods are in very good agreement. From Fig. 3.7(d), we find that the excitation probability of the second qubit calculated via the cost function shows very good agreement with the analytical solution [see Eq. (3.18)]. With this, we have verified that the cost function can be converted to the excitation of the second qubit via Eq. (3.39) within the Wigner-Weisskopf approximation. Also, the Wigner-Weisskopf results agree very well with the result obtained via ED.

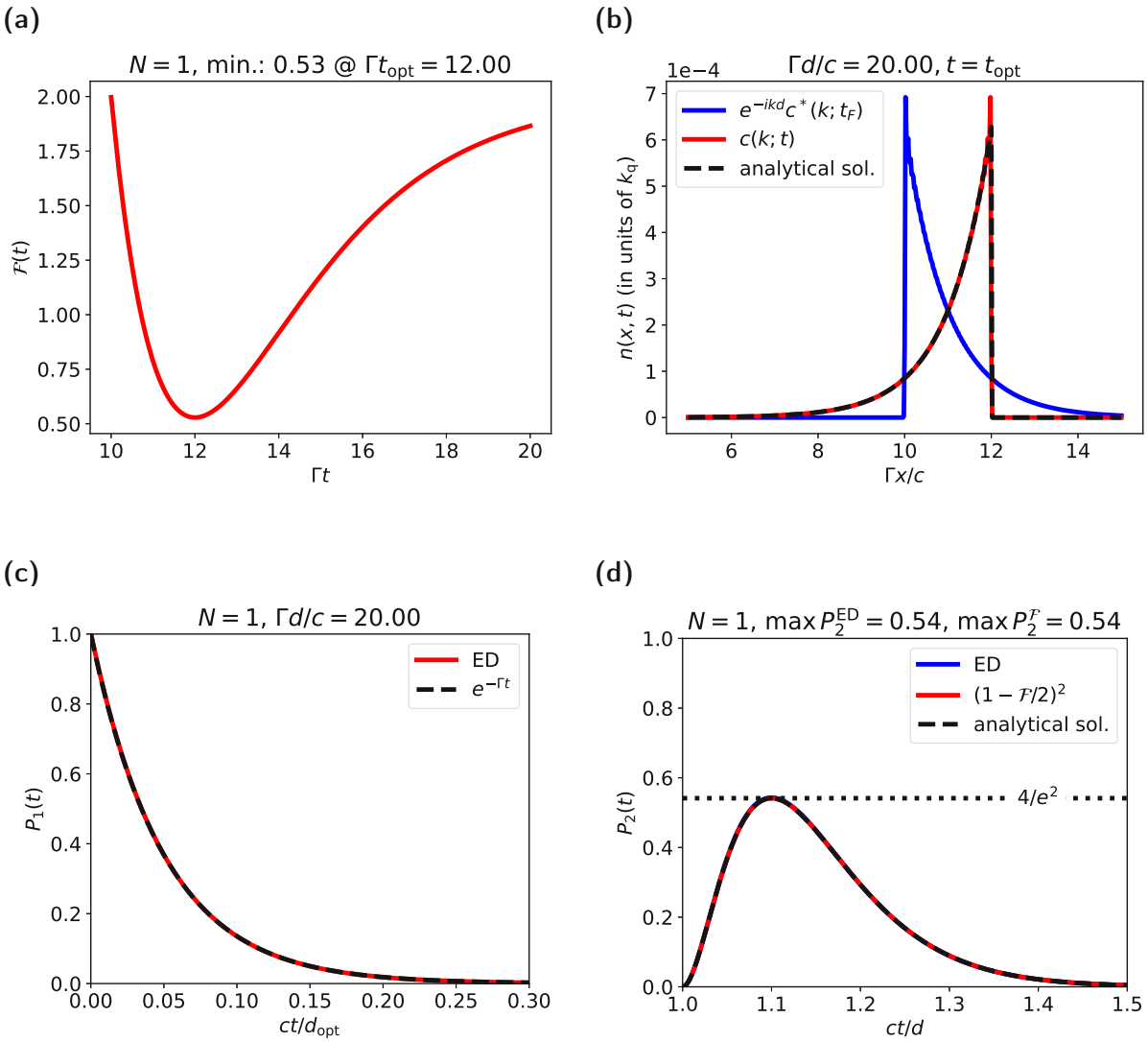

Figure 3.7: (a) Cost function and (b) pulse overlap in position space for a linear dispersion. The red curve in plot (b) corresponds to the time-evolved emitted pulse, the blue curve is the target pulse and the black dashed curve is the analytical solution for the pulse. (c) Time evolution of the excitation probability of the first qubit calculated via ED (red curve) and Wigner-Weisskopf theory (black dashed curve). (d) Excitation probabilities of the second qubit obtained via the cost function (red curve) and via ED (blue curve) compared to the analytical solution (black dashed curve).

4 Results

In this chapter, we apply our pulse overlap method developed in the previous sections to a system of two qubits chirally coupled to a 1D waveguide. First, we specifically discuss the results for a dispersion relation of polynomial degree $N = 3$, in particular the parameter combinations' behaviour. Following this analysis, we focus on the results for dispersion relations of higher polynomial degrees $N > 3$. The results are compared to the solutions obtained via ED.

4.1 Dispersion relation of polynomial degree three

First, we want to look at the results for a polynomial dispersion relation of degree $N = 3$, because in this case we can study the parameter combinations of a_2 and a_3 for different qubit separations. For higher polynomial degrees, the parameter behaviour is more complicated to interpret. The dispersion relation [see Eq. (3.20)] for degree $N = 3$ reads

$$\begin{aligned}\omega(k) - \omega_\mathrm{q} &= \omega_\mathrm{q}\xi \frac{(\xi - z)(\xi - z^*)}{|z|^2} \\ &= \omega_\mathrm{q}\xi \left(1 - \frac{2z_r\xi}{|z|^2} + \frac{\xi^2}{|z|^2}\right) \\ &= \omega_\mathrm{q} \sum_{n=1}^{3} a_n \xi^n, \quad \text{with} \quad \xi \equiv \frac{k - k_\mathrm{q}}{k_\mathrm{q}}.\end{aligned} \tag{4.1}$$

From Eq. (4.1), we can directly deduce the parameters, which are given by

$$\begin{aligned} a_1 &= 1, \\ a_2 &= -\frac{2z_r}{z_r^2 + z_i^2}, \\ a_3 &= \frac{1}{z_r^2 + z_i^2}. \end{aligned} \tag{4.2}$$

In Fig. 4.1, we show the parameter combinations a_2, a_3 and the corresponding minima of the cost function as a function of the qubit separation d. We remind ourselves, that the minimum of the cost function refers to the smallest minimum of the cost function achieved over the optimizations for all initial parameter sets (see Sec. 3.4.3).

We observe that the parameter values for a_2 and a_3 vary significantly for qubit separations up to $\Gamma d/c \approx 500$. For larger separations $500 \lesssim \Gamma d/c \lesssim \Gamma d_\mathrm{opt}/c$, the

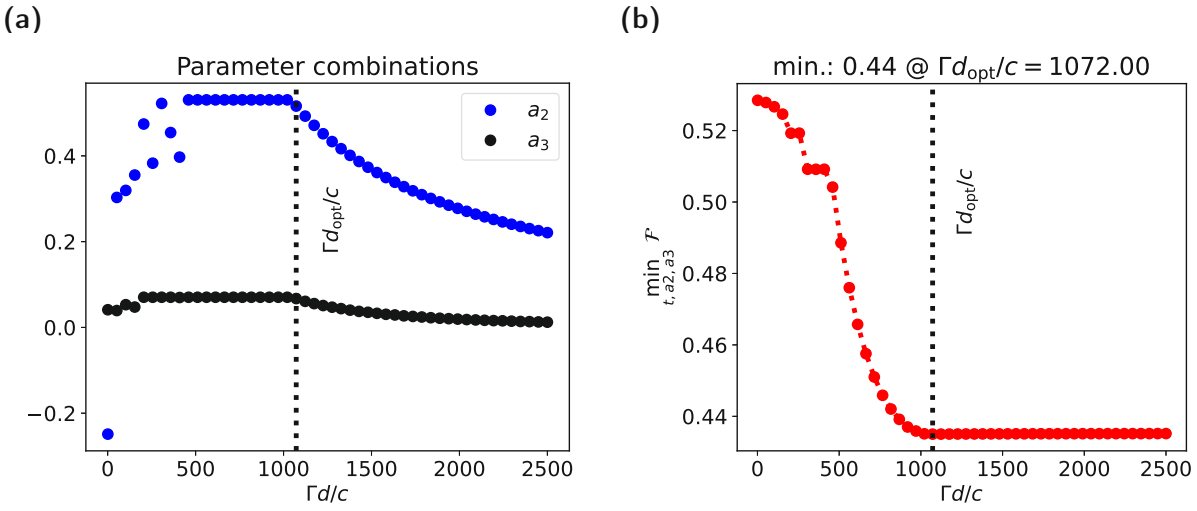

Figure 4.1: (a) Parameter combinations of a_2, a_3 and (b) minima of the cost function for different qubit separations d. In plot (a), the vertical black dotted line corresponds to the optimal qubit separation d_{opt}. Results are obtained via optimization for polynomial degree $N = 3$ and $n_s = 10^5$ initial Monte Carlo sampled parameter sets (see Sec. 3.4.3).

parameters tend to stay at a constant value. Here, d_{opt} is the separation, where we first reach the smallest minimum of the cost function [see Fig. 4.1(b)]. This minimum will be referred to as "optimal minimum of the cost function" and the corresponding qubit separation will be referred to as "optimal qubit separation". In this region, the minimum of the cost function steadily decreases for increasing d. Near the optimal qubit separation, $d \approx d_{\text{opt}}$, the parameter curves for a_2 and a_3 show a kink and then the values tend to decrease for increasing d. For very large separations, the general trend seems to be that the parameters a_2 and a_3 fall together at a small finite value. This behaviour can be explained as follows. At the optimal qubit separation, the single-photon pulse reaches its "optimal shape", i.e. it cannot have a better shape for absorption. If the separation between the qubits is further increased, the pulse takes longer to deform to its optimal shape according to the dispersion relation. The "deformation speed" is governed by the parameters a_2 and a_3 in the dispersion relation. Thus, for increasing qubit separations, the values for a_2 and a_3 decrease. For very large qubit separations, a_2 and a_3 are very small, i.e. the dispersion relation is weakly non-linear.

Importantly, we find that the optimal minimum of the cost function in Fig. 4.1(b) corresponds to a maximum excitation probability [see Eq. (3.39)]

$$\max P_2^{(3)}(t) = \left\{1 - \frac{1}{2} \min_d \left[\min_{t,a_2,a_3} \mathcal{F}(t)\right]\right\}^2 \approx 0.61 \tag{4.3}$$

of the second qubit. This is significantly higher ($\approx 7\%$) than in the case of a linear dispersion relation, where we have $\max P_2^{\text{lin}}(t) = 4/e^2 \approx 0.54$ (see Sec. 3.1.2).

In Fig. 4.2, we show the cost function and the pulse overlap in position space for the optimal qubit separation d_{opt}. The pulse overlap in position space is shown for the optimal

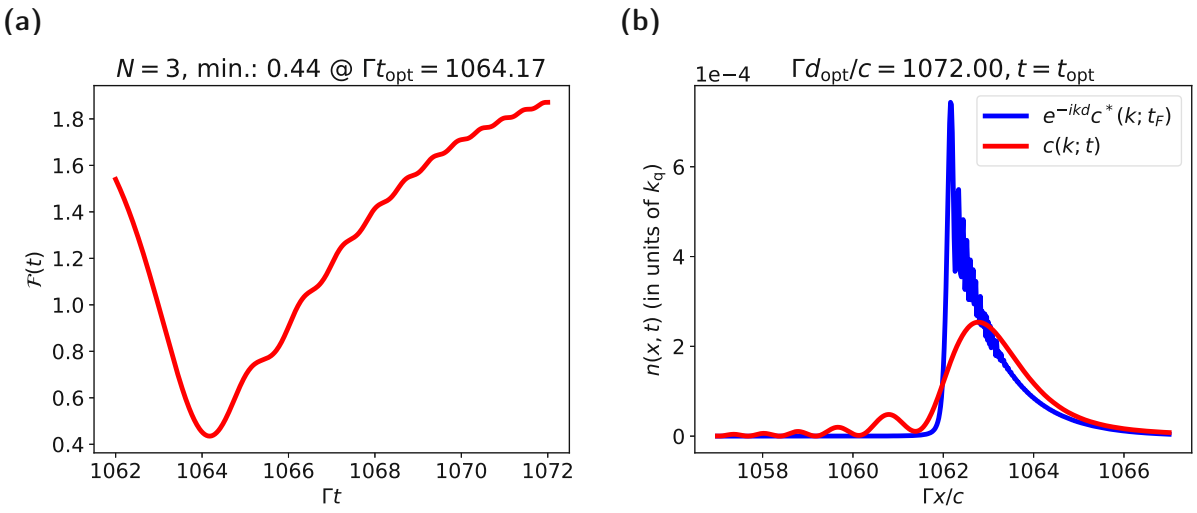

Figure 4.2: (a) Cost function and (b) pulse overlap in position space for the optimal qubit separation d_{opt}. The red curve in plot (b) corresponds to the time-evolved emitted pulse and the blue pulse is the target pulse. Results are obtained via optimization for polynomial degree $N = 3$ and $n_s = 10^5$ initial Monte Carlo sampled parameter sets (see Sec. 3.4.3).

time. We observe, that the cost function[1] is a smooth function with possibly local minima on the right hand side, which justifies using Monte Carlo sampling in time. Further, the deformed pulse mimics the shape of the target pulse, i.e. the time-reversed single-photon pulse.

In Fig. 4.3, we plot the dispersion relation for the optimal minimum of the cost function and the corresponding emission spectrum for the optimal time.

We find, that the dispersion relation intersects the qubit transition frequency at $k = k_{\text{q}}$, which we demanded a priori by the construction of the dispersion relation [see Eq. (3.20)] and the root constraints (see Sec. 3.4.2). Also, in Fig. 4.3(b), we see, that the spectrum is sharply peaked around $k = k_{\text{q}}$ with no secondary peaks, i.e. we have only one emission channel for the qubit. Further, the Lorentzian shows small deviations from zero towards zero momentum, but it has decayed to less than 0.1% of its maximum height, which we demanded a priori (see Sec. 3.4.2). Also, the probability is conserved up to an absolute error of $\approx 0.2\%$ (see Appendix B).

For verification, we use exact diagonalization (ED) to calculate the time evolution of the full two-qubit system (see Sec. 3.5.1) for the obtained set of optimization parameters $\{t; z_r; z_i\}$, with z_r and z_i being the real and imaginary part of the complex root of the detuning, respectively.

In Fig. 4.4, we show the time evolution of the qubit excitation probabilities calculated with ED for the optimal qubit separation. Also, we compare the excitation probabilities of the second qubit calculated via the cost function and ED, as well as for a linear dispersion relation [see Eq. (3.18)], respectively.

[1] For numerical convergence checks on the cost function see Appendix A.

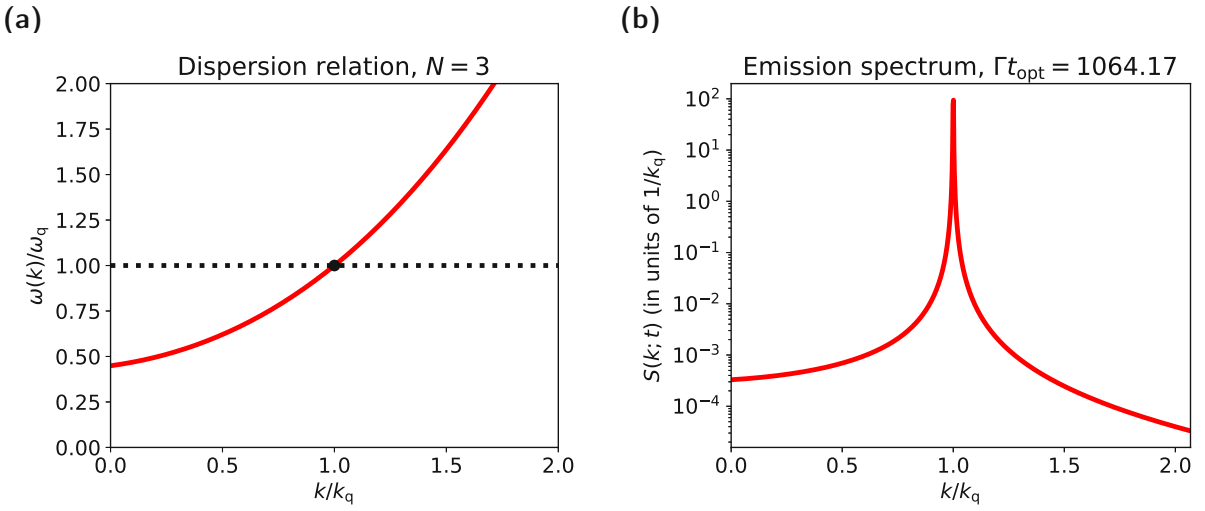

Figure 4.3: (a) Optimal dispersion relation and (b) emission spectrum at the optimal time t_{opt}. In the dispersion plot (a), the qubit transition frequency ω_q is depicted as a black dotted line. The black dot is the intersection point of the band and the qubit transition frequency at $k = k_q$. Results are obtained via optimization for polynomial degree $N = 3$ and $n_s = 10^5$ initial Monte Carlo sampled parameter sets (see Sec. 3.4.3).

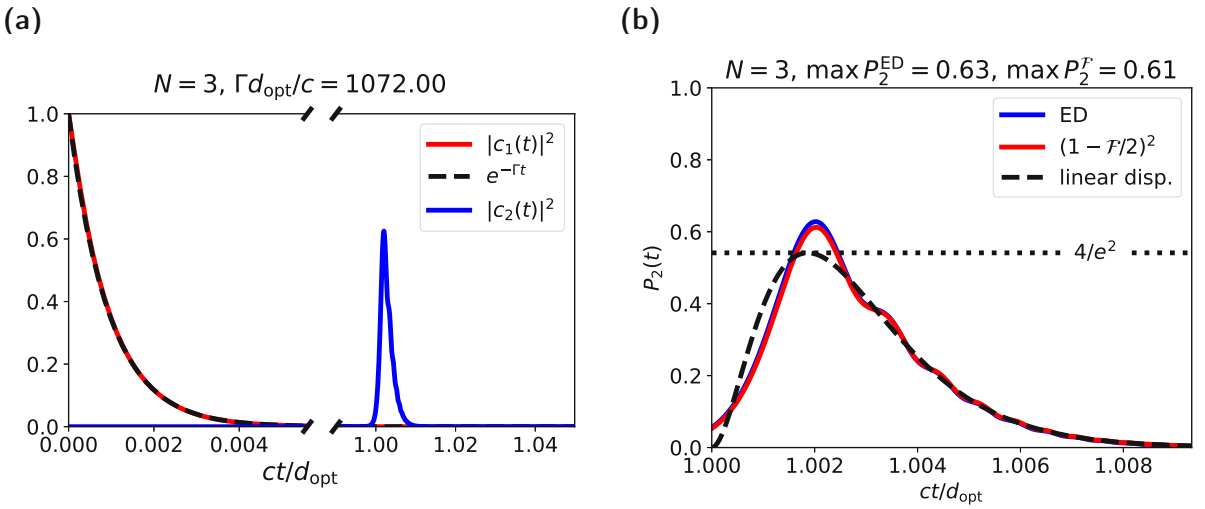

Figure 4.4: (a) Time evolution of the qubit excitation probabilities calculated via exact diagonalization for the optimal qubit separation. (b) Comparison of the excitation probability of the second qubit obtained via converting the cost function (red curve) and via ED (blue curve). The black dashed curve shows the analytical solution for a linear dispersion relation. The optimization was run for polynomial degree $N = 3$ and $n_s = 10^5$ initial Monte Carlo sampled parameter sets (see Sec. 3.4.3).

We find, that the excitation probabilities of the second qubit calculated via ED and Wigner-Weisskopf theory show a deviation at the peak of $\approx 2\%$. This deviation is caused by the finite discretization in ED combined with the chirality of the waveguide.

4.2 Dispersion relations of higher polynomial degrees

Now, we want to approach dispersion relations of higher polynomial degrees N in order to study the maximum excitation of the second qubit and the optimal qubit separation d_{opt} in those cases. Higher polynomial degrees lead to a larger number of parameters to modify the dispersion relation shape, which could be beneficial for the single-photon absorption. On the other hand, the numerical optimization complexity increases with the polynomial degree[2].

In Figs. 4.5 and 4.6, we plot the minima of the cost function[3] over the qubit separation for the polynomial degrees $N = 3$ to $N = 13$ and $N = 15$ to $N = 25$, respectively. We can observe, that the optimal qubit separation d_{opt} decreases for increasing polynomial degrees N, but the optimal minimum of the cost function does not seem to decrease significantly. Also, the curves are not smooth over the whole range, i.e. there are points that have not converged in the optimization. Thus, the number of initial Monte Carlo samples (i.e. sampled parameter sets) would have to be increased even further. Because of the computational limitations, this could not be realized. On the other hand, with the current results, we can observe the overall trend and especially the optimal minima are surely well captured (see smoothness of curves for distances $d \geq d_{\text{opt}}$). This is important, because the optimal minima represent the optimal pulse overlap and thus the maximum absorption of the photon by the second qubit.

In Fig. 4.7, we plot the dispersion relation corresponding to the optimal minimum of the cost function and the emission spectrum for the optimal time for different polynomial degrees. We again find, that the dispersion relation intersects the qubit transition frequency at $k = k_{\text{q}}$, which was demanded a priori. For increasing polynomial degrees the band comes closer to the transition frequency ω_{q} towards zero momentum within the given constraints. This is because multiple emission channels would allow for more degrees of freedom in the optimization. Also, in Fig. 4.7(b), we see, that the spectrum is sharply peaked around $k = k_{\text{q}}$ with no secondary peaks for the selected polynomial degrees. This verifies, that we indeed have only one emission channel for the qubit. Further, the Lorentzians are very similar and small deviations from zero away from the resonance become visible only on a log-scale. The Lorentzians have decayed to less than 0.1% of their maximum height, which we demanded a priori (see Sec. 3.4.2). Also, the probability is conserved up to an absolute error of around 0.2% (see Appendix B). All other probed degrees show very similar results regarding the spectrum.

For verification, we again use exact diagonalization to calculate the time evolution of the full two-qubit system (see Sec. 3.5.1) for the obtained set of optimization parameters $\{t; z_{1,r}, \ldots, z_{n,r}; z_{1,i}, \ldots, z_{n,i}\}$, where n is the number of complex roots of the detuning.

[2]The cost function has to be minimized over a parameter set $\{t; z_{1,r}, \ldots, z_{n,r}; z_{1,i}, \ldots, z_{n,i}\}$, which has exactly N parameters. The polynomial degree N thus directly determines the number of optimization parameters.

[3]For numerical convergence checks on the cost functions see Appendix A.

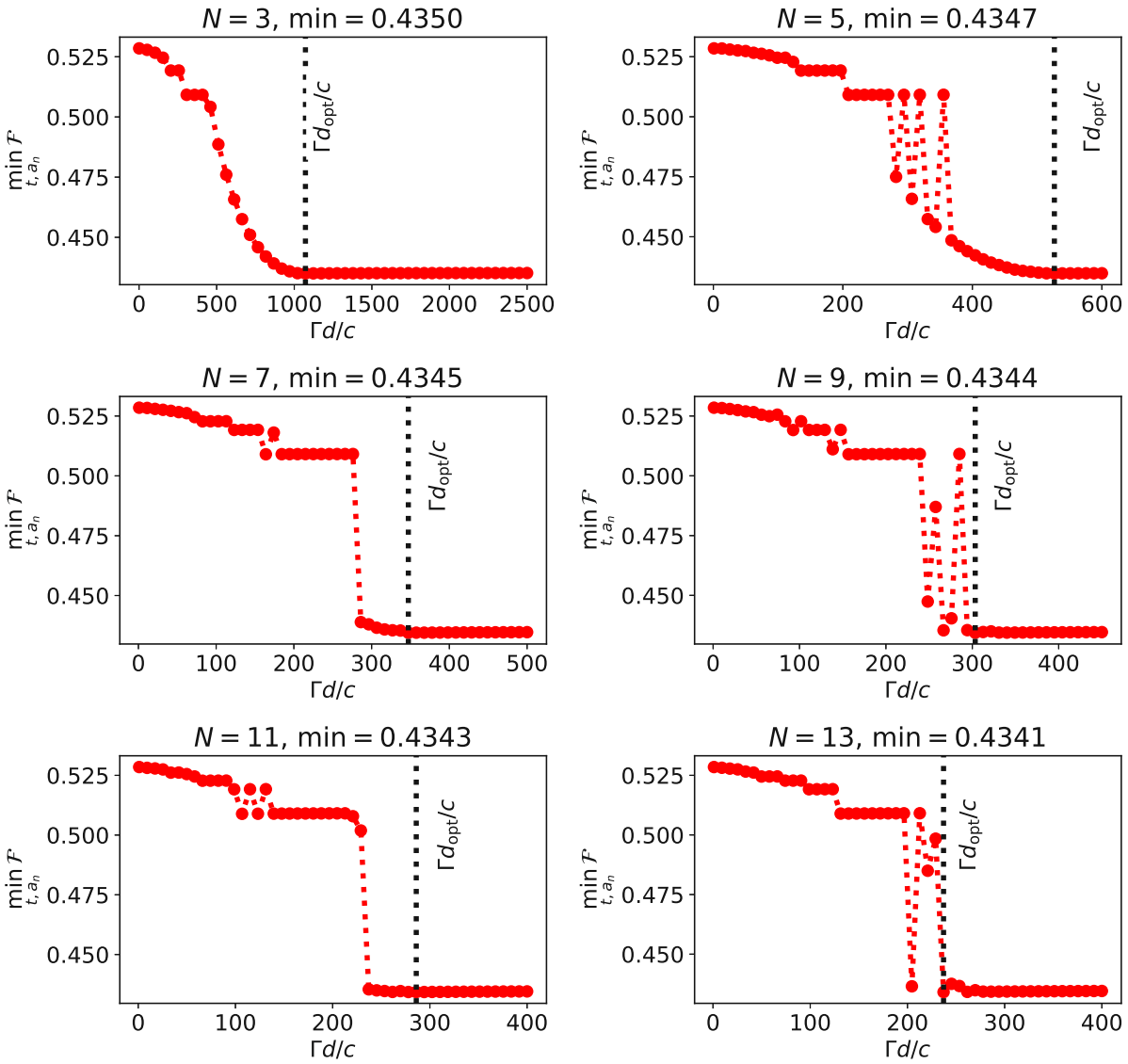

Figure 4.5: Minima of the cost function for different qubit separations d and polynomial degrees $N = 3$ to $N = 13$. Results are obtained via optimization for $n_s = 1.8 \cdot 10^5$ ($n_s = 1 \cdot 10^5$ for $N = 3$) initial Monte Carlo sampled parameter sets (see Sec. 3.4.3). Note that the x-axis changes between some polynomial degrees.

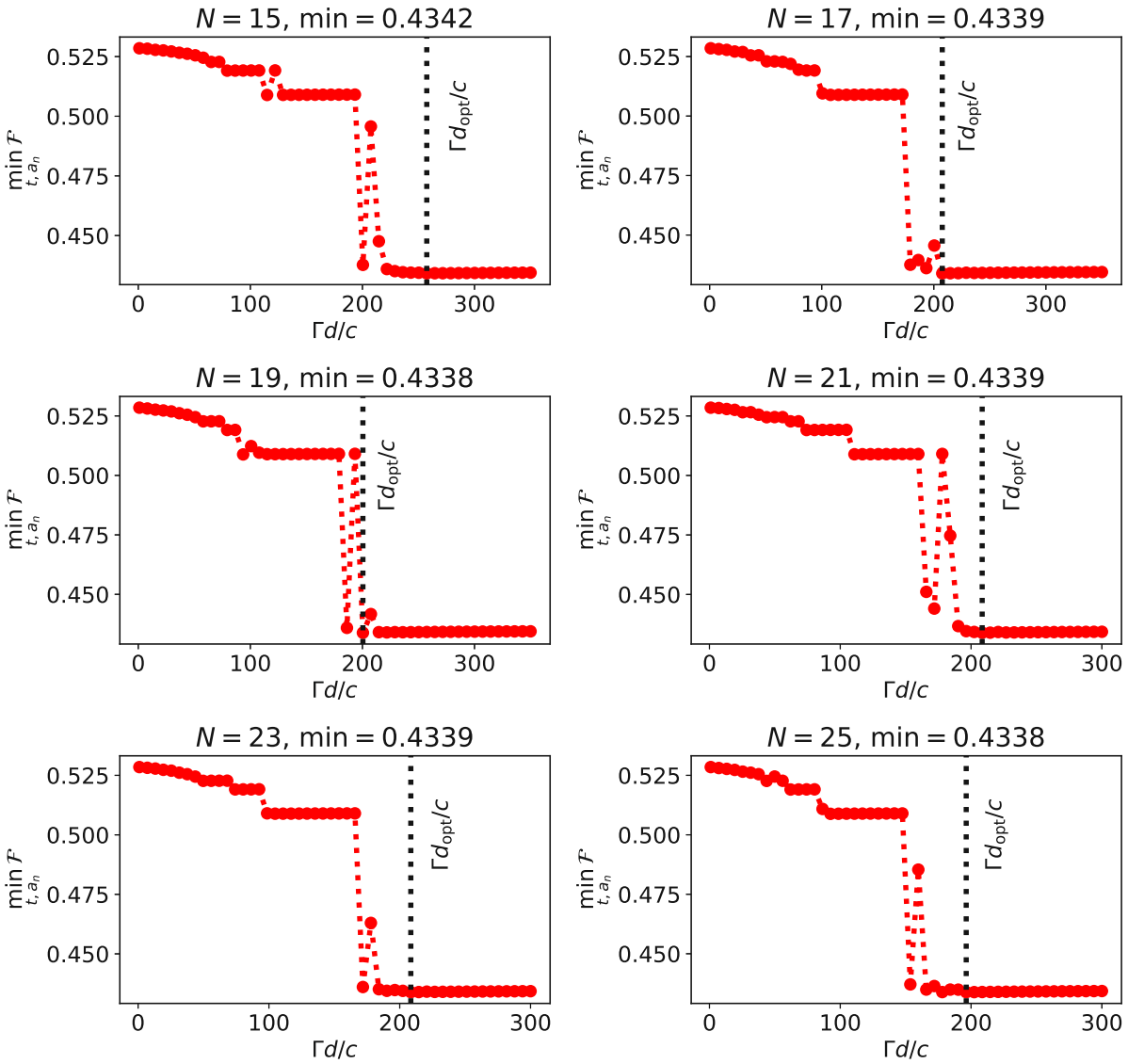

Figure 4.6: Minima of the cost function for different qubit separations d and polynomial degrees $N = 15$ to $N = 25$. Results are obtained via optimization for $n_s = 1.8 \cdot 10^5$ initial Monte Carlo sampled parameter sets (see Sec. 3.4.3). Note that the x-axis changes between some polynomial degrees.

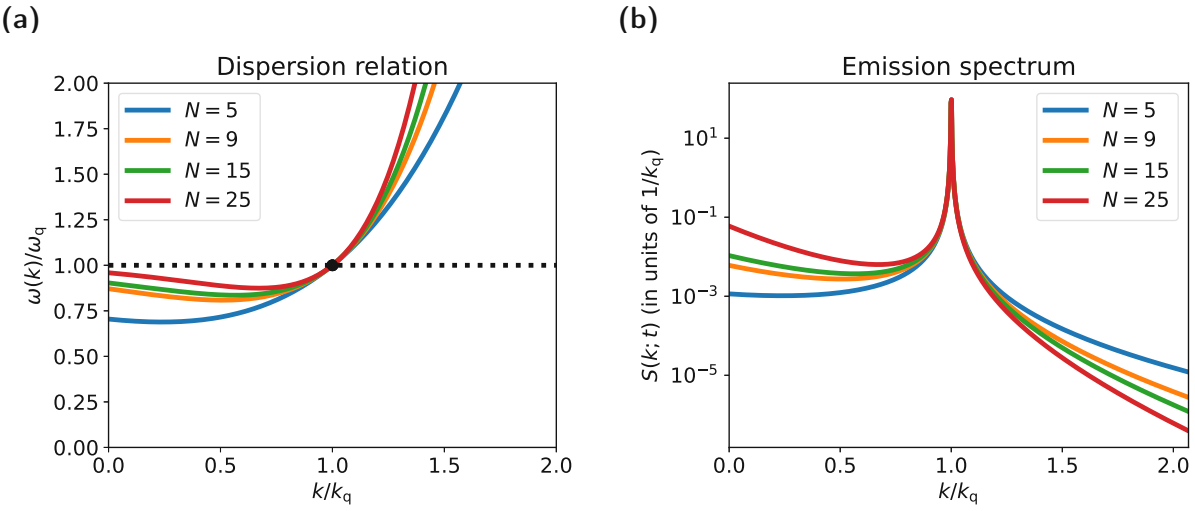

Figure 4.7: (a) Optimal dispersion relation and (b) emission spectrum at the optimal time t_{opt} for different polynomial degrees N. In the dispersion plot (a), the qubit transition frequency ω_q is depicted as a black dotted line. The black dot is the intersection point of the band and the qubit transition frequency at $k = k_q$. Results are obtained via optimization for $n_s = 1.8 \cdot 10^5$ initial Monte Carlo sampled parameter sets (see Sec. 3.4.3).

In Figs. 4.8, 4.9 and 4.10, we plot the cost function and the pulse overlap in position space for the optimal qubit separation d_{opt} for the polynomial degrees $N = 5$, $N = 15$ and $N = 25$, respectively. For the same degrees, we also show the time evolution of the qubit excitation probabilities, calculated with ED, for the optimal qubit separation. Additionally, we compare the excitation probabilities of the second qubit calculated via the cost function and ED, as well as for a linear dispersion, respectively. For the selected polynomial degrees, the pulse overlap results are very similar to the ones for polynomial degree $N = 3$ apart from a slightly better pulse overlap. The excitation probabilities of the second qubit calculated via ED and Wigner-Weisskopf theory show a deviation at the peak of $\approx 2\%$. This deviation is caused by the finite discretization in ED combined with the chirality of the waveguide.

In Fig. 4.11, we plot the optimal qubit separations d_{opt}, the optimal minima of the cost function and the corresponding maximum excitation probabilities of the second qubit (calculated via the converted cost function and via ED) as a function of the polynomial degree. The maximum excitation probability of the second qubit for a specific polynomial degree N is given by [see Eq. (3.39)]

$$\max P_2^{(N)}(t) = \left\{1 - \frac{1}{2} \min_d \left[\min_{t,a_n} \mathcal{F}(t)\right]\right\}^2 . \tag{4.4}$$

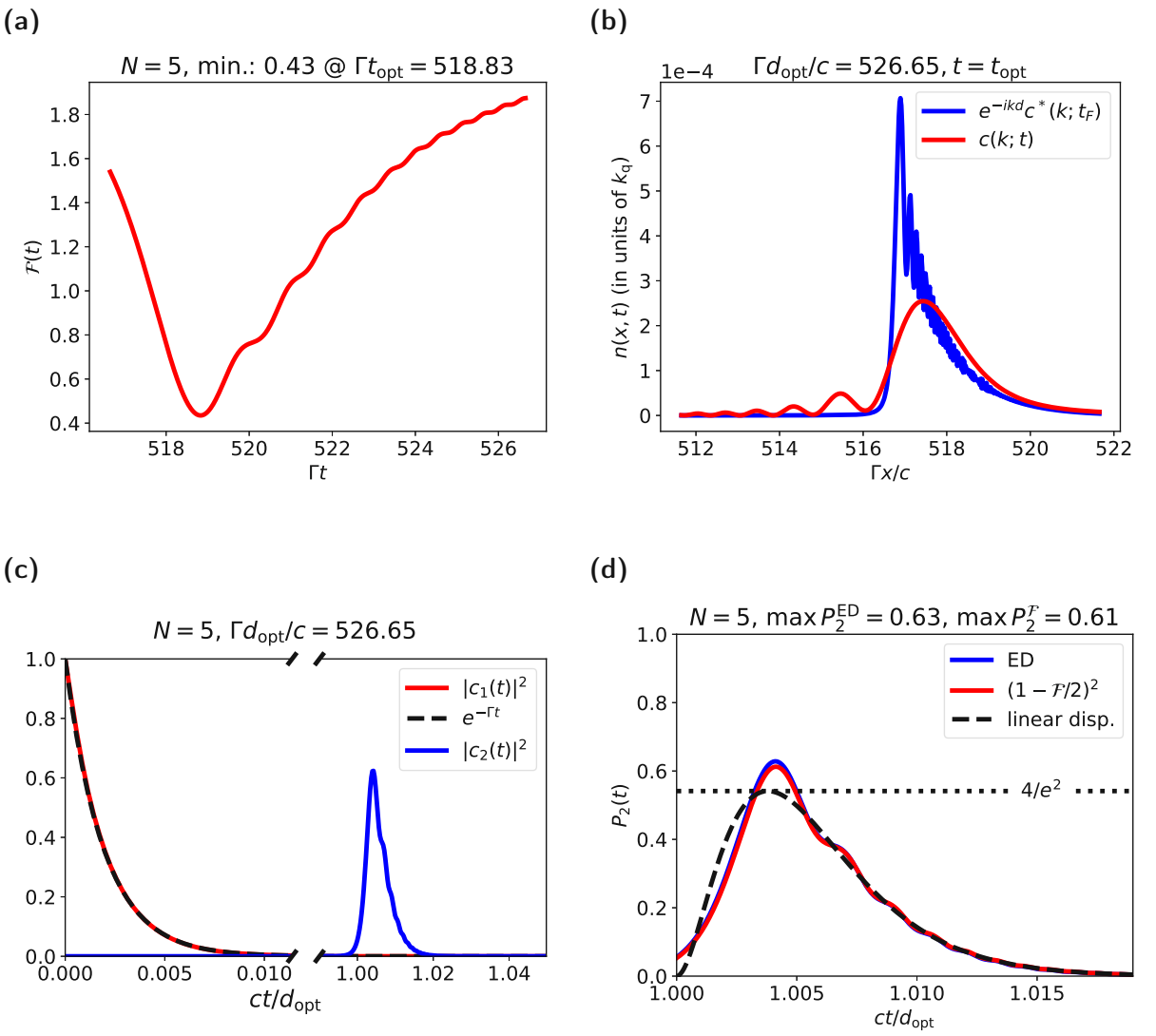

Figure 4.8: (a) Cost function and (b) pulse overlap in position space for the optimal qubit separation d_{opt}. The red curve in plot (b) corresponds to the time-evolved emitted pulse and the blue pulse is the target pulse. (c) Time evolution of the qubit excitation probabilities calculated via exact diagonalization for the optimal qubit separation. (d) Comparison of the excitation probability of the second qubit obtained via converting the cost function (red curve) and via ED (blue curve). The black dashed curve shows the analytical solution for a linear dispersion relation. The optimization was run for polynomial degree $N = 5$ and $n_s = 1.8 \cdot 10^5$ initial Monte Carlo sampled parameter sets (see Sec. 3.4.3).

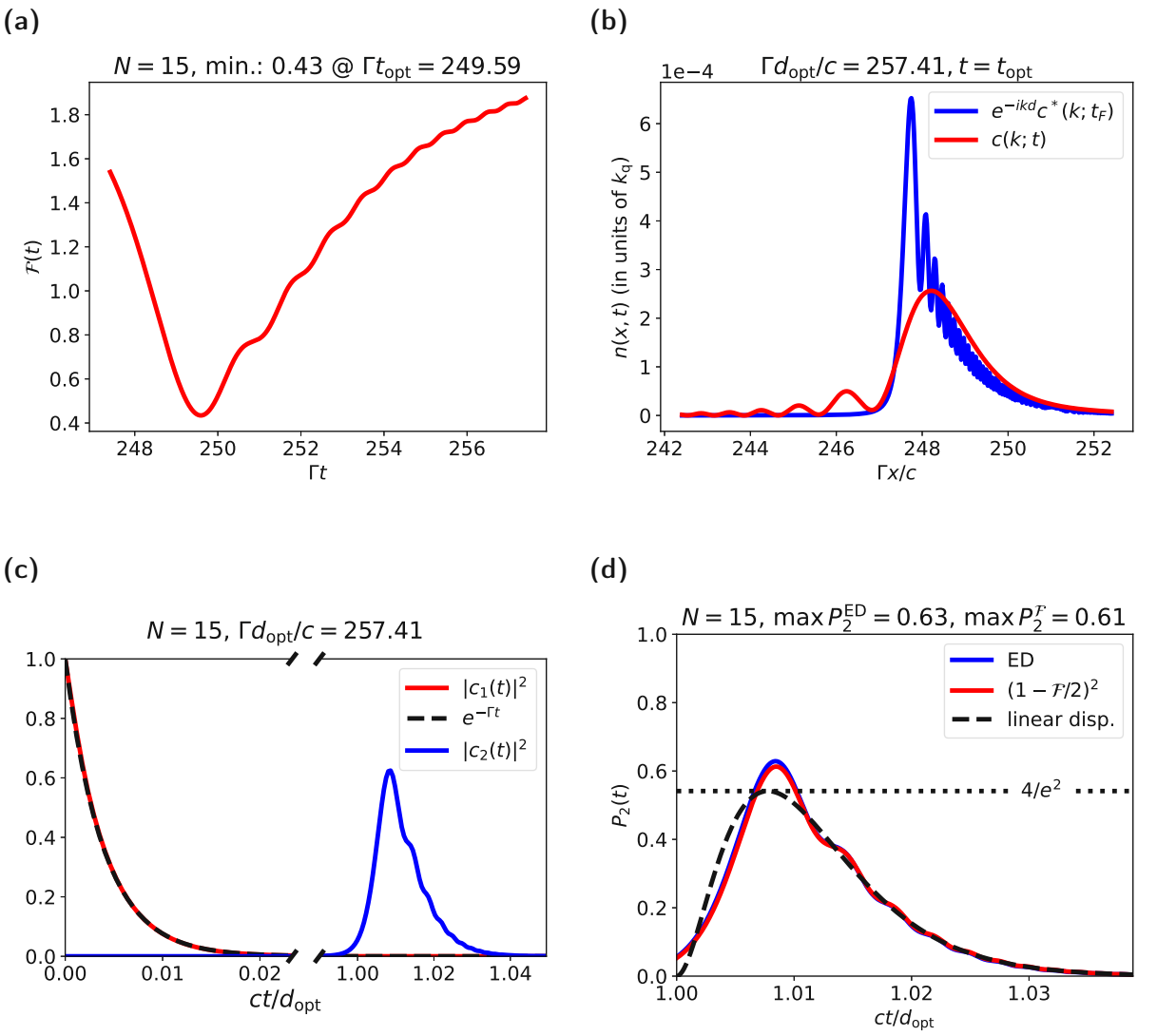

Figure 4.9: (a) Cost function and (b) pulse overlap in position space for the optimal qubit separation d_{opt}. The red curve in plot (b) corresponds to the time-evolved emitted pulse and the blue pulse is the target pulse. (c) Time evolution of the qubit excitation probabilities calculated via exact diagonalization for the optimal qubit separation. (d) Comparison of the excitation probability of the second qubit obtained via converting the cost function (red curve) and via ED (blue curve). The black dashed curve shows the analytical solution for a linear dispersion relation. The optimization was run for polynomial degree $N = 15$ and $n_s = 1.8 \cdot 10^5$ initial Monte Carlo sampled parameter sets (see Sec. 3.4.3).

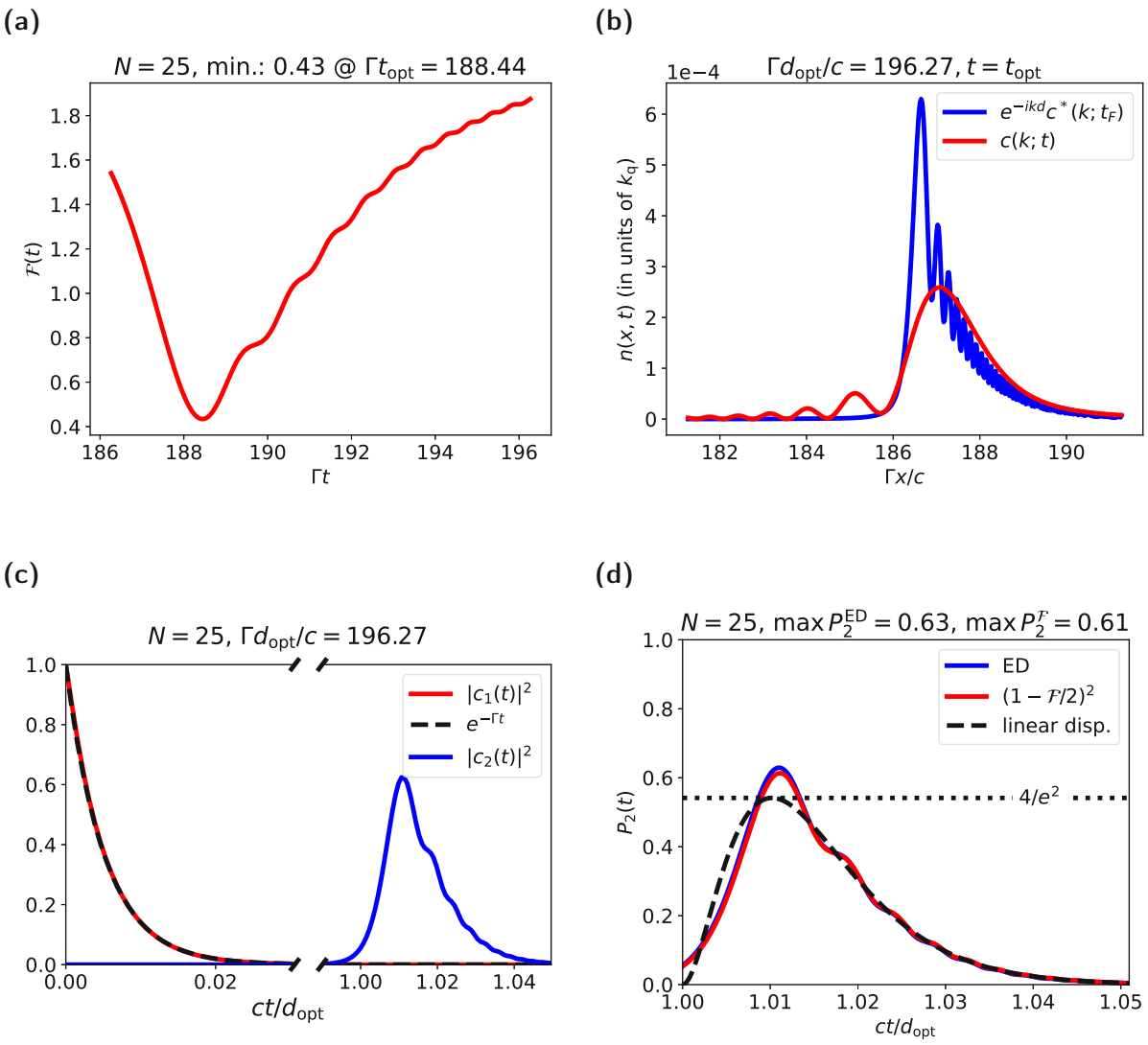

Figure 4.10: (a) Cost function and (b) pulse overlap in position space for the optimal qubit separation d_{opt}. The red curve in plot (b) corresponds to the time-evolved emitted pulse and the blue pulse is the target pulse. (c) Time evolution of the qubit excitation probabilities calculated via exact diagonalization for the optimal qubit separation. (d) Comparison of the excitation probability of the second qubit obtained via converting the cost function (red curve) and via ED (blue curve). The black dashed curve shows the analytical solution for a linear dispersion relation. The optimization was run for polynomial degree $N = 25$ and $n_s = 1.8 \cdot 10^5$ initial Monte Carlo sampled parameter sets (see Sec. 3.4.3).

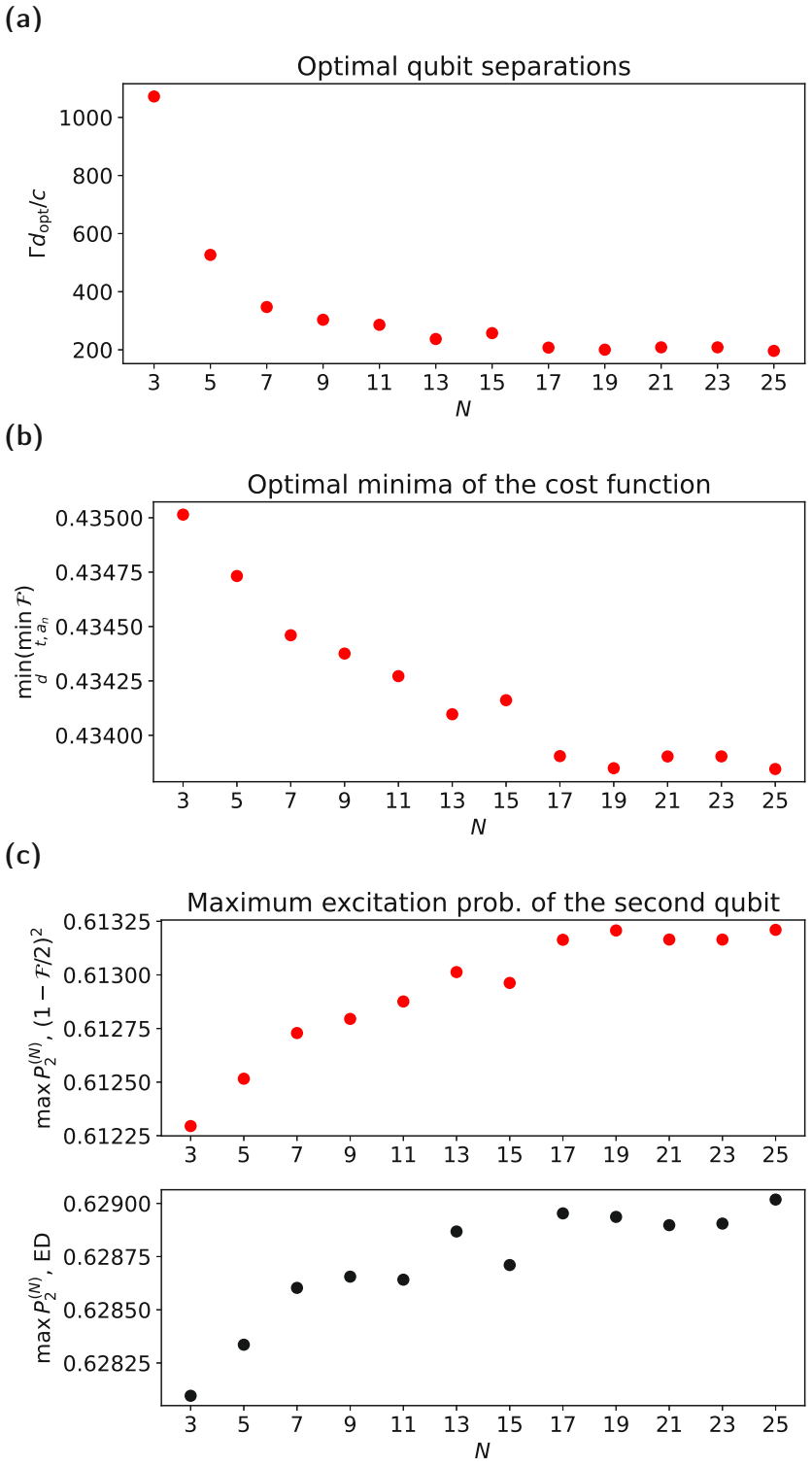

Figure 4.11: (a) Optimal qubit separations, (b) optimal minima of the cost function and (c) maximum excitation probabilities of the second qubit calculated via the cost function (upper plot) and via ED (lower plot) as a function of the polynomial degree N. Results are obtained via optimization for $n_s = 1.8 \cdot 10^5$ ($n_s = 10^5$ for $N = 3$) initial Monte Carlo sampled parameter sets (see Sec. 3.4.3).

Fig. 4.11(a) shows that the optimal qubit separation decreases for increasing polynomial degrees, where the shift towards smaller separations is bigger for lower degrees. From Fig. 4.11(b), we find that the optimal minimum of the cost function, which determines the maximum excitation probability of the second qubit, steadily decreases for increasing polynomial degrees apart from a few fluctuations. In Fig. 4.11(c), we can observe that the maximum excitation probabilities calculated via the two methods show a similar trend with an overall increase of the single-photon absorption by $\approx 0.1\%$. The results for the two methods show deviations of $\approx 2\%$. As previously mentioned, this deviation is caused by a combination of the effects due to the finite discretization in ED and the chiral couplings. It is important to note, that the results in each curve in Figs. 4.11(b) and 4.11(c) remain below the accuracy of the probability conservation, which is $\approx 0.2\%$ (see Appendix B). Thus, the results are not completely conclusive.

From the results, we can deduce, that a non-linear dispersion relation indeed increases the excitation probability of the second qubit, i.e. the single-photon absorption by a second qubit in the waveguide is improved. The increase compared to a linear dispersion is $\approx 7\%$. What we also find is, that by increasing the polynomial degree, the optimal qubit separation is significantly reduced. We ascribe the saturation of the transfer – which cannot get better than $\approx 61\%$ – to the fact that our exploration remains within parameter values consistent with the Markov approximation. Within this approximation the allowed dispersion relations are very restricted, preventing from modifying the initial single-photon pulse in momentum space into the most optimal shape. Exploring non-Markovian regimes is a potential outlook of this work.

5 Conclusion and Outlook

The perfect transfer of single photons in quantum systems has many promising applications in quantum information and communication. Waveguide QED setups serve as promising platforms in this context. In a standard waveguide, perfect excitation of a qubit by a spontaneously emitted single photon is not possible due to the emission in all directions of the waveguide. An alternative is to study chiral waveguides, where the photon emission becomes unidirectional. For a linear dispersion relation in the waveguide, the single-photon absorption has a fundamental limit of around 54% [22].

In this thesis, we investigated the single-photon transfer between two identical qubits, which are chirally coupled to a 1D photonic waveguide. In order to improve the transfer of a spontaneously emitted single photon between the two qubits in a chiral waveguide, we engineered non-linear dispersion relations to reshape the single-photon pulse in such a way, that it mimics the time-reversed version of the initial pulse. Due to the time-reversal symmetry of the Schrödinger equation, the time-reversed version of the spontaneously emitted photon can be perfectly absorbed by the second qubit. We constructed the non-linear dispersion relation, such that all calculations and numerical simulations are consistent within Wigner-Weisskopf theory, i.e. within the Markov regime. On that basis, we introduced an optimization method, where the spatial overlap between the propagating single-photon pulse, which is deformed according to the dispersion relation, and the time-reversed single-photon pulse is maximized.

Our method to optimize the single-photon transfer between two qubits was confirmed by means of analytical calculations and complementary numerical simulations.

We could show, that by engineering non-linear dispersion relations in a 1D chiral waveguide, the single-photon absorption by a second qubit is indeed improved. The increase compared to a linear dispersion relation is $\approx 7\%$. By studying dispersion relations of higher polynomial degrees, we found that the maximum excitation of the second qubit cannot be increased further within the Markov regime. However, we found that the distance between the two qubits, where the maximum absorption occurs, decreases for increasing polynomial degrees. This allows for a more flexible qubit placement for dispersion relations of higher order.

The method presented in this thesis serves as a first step towards achieving perfect single-photon transfer between two qubits. Although we could not achieve perfect single-

photon transfer in a dispersion-engineered 1D chiral waveguide, we found significant improvement over a linear dispersion relation, i.e. we could shape the single-photon pulse, such that it mimics the time-reversed initial pulse. From the results, we can deduce that within the Markov regime perfect single-photon transfer seems unlikely because of the required constraints on the dispersion relation and the single-photon pulse. Preliminary results already suggest, that the absorption is greatly enhanced by leaving the Markov regime. Thus, in future research, it will be beneficial to explore the non-Markovian regime in order to achieve a more efficient (or even perfect) single-photon transfer.

Appendix A

Numerical Convergence

In order to quantify the convergence of the numerical integrations involved in various calculations, we look at the error between two consecutive iterations of results obtained through numerical integrations as a function of the iteration number and the integration stepsize, respectively. Here, one iteration corresponds to one numerical integration for a fixed stepsize on the k-axis. After each iteration, the stepsize, Δk, is decreased by a factor of $\kappa < 1$, i.e. $(\Delta k)_{i+1} = \kappa \cdot (\Delta k)_i$, where i is the iteration number. We quantify the numerical error through the maximum norm, i.e. the error at a specific iteration is given by

$$\mathcal{E}_i = ||f_i - f_{i-1}||_\infty, \tag{A.1}$$

with $||f||_\infty := \max_{x_n \in I} |f(x_n)|$.

In Figs. A.1 and A.2, we show the numerical convergence of the cost function, quantified by the error $\mathcal{E}_i = ||\mathcal{F}_i - \mathcal{F}_{i-1}||_\infty$, for $\kappa = 0.6$, 15 iterations and various polynomial degrees. The initial stepsize is $(\Delta k)_0/k_\mathrm{q} = 1 \cdot 10^{-3}$. In all calculations, we use a coupling strength of $g_0/\sqrt{\omega_\mathrm{q} c} = 0.01$. We observe, that the cost function converges nicely for decreasing stepsize Δk for all selected polynomial degrees. For the stepsize we are working with in the calculations, $\Delta k/k_\mathrm{q} = 5 \cdot 10^{-6}$, we have a numerical error of $\mathcal{E} \approx \mathcal{E}_{11} \approx 1 \cdot 10^{-8}$.

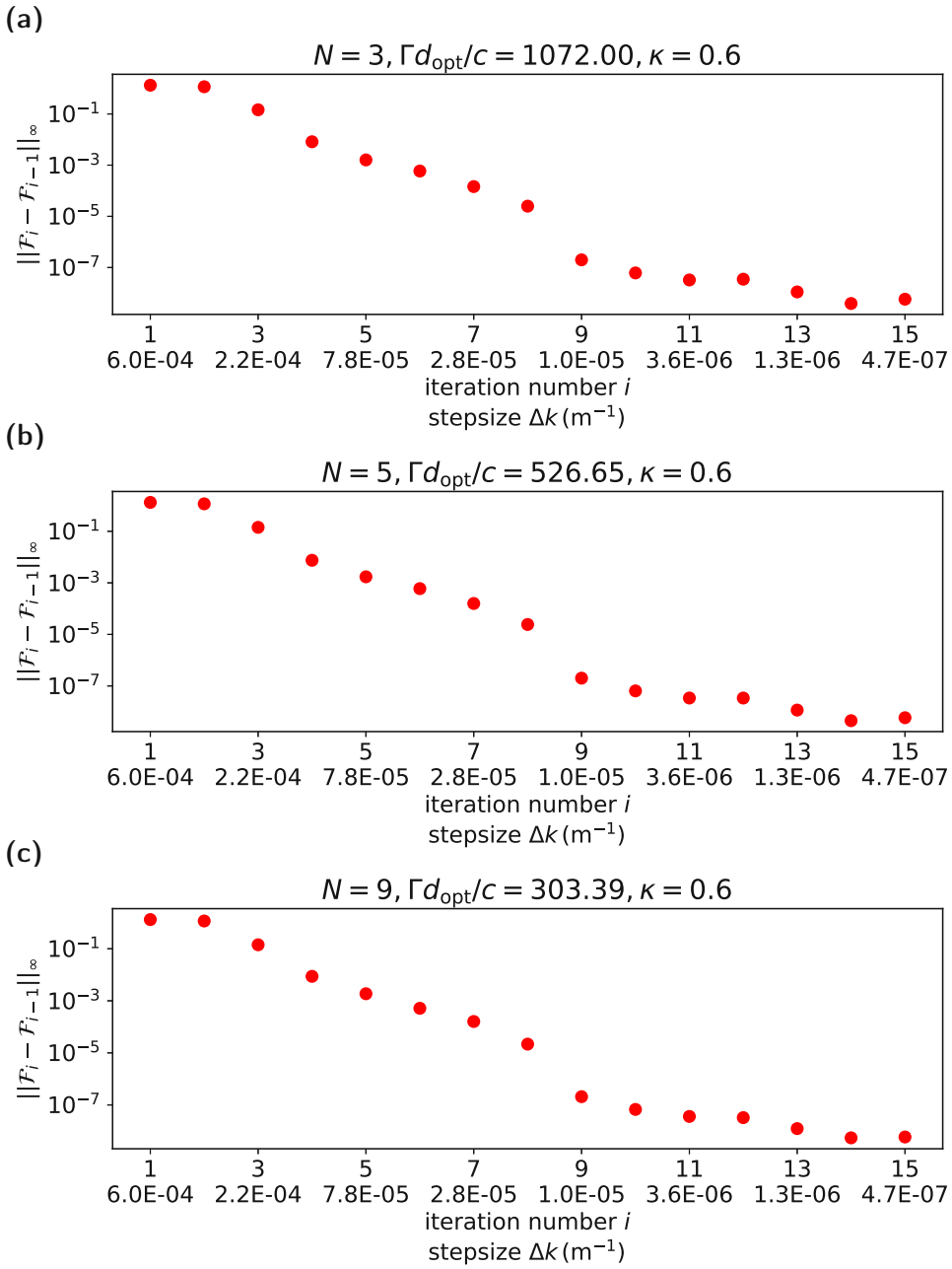

Figure A.1: Numerical convergence of the cost function for the optimal dispersion relation (see Secs. 4.1 and 4.2). Example results are shown for polynomial degree (a) $N = 3$, (b) $N = 5$ and (c) $N = 9$.

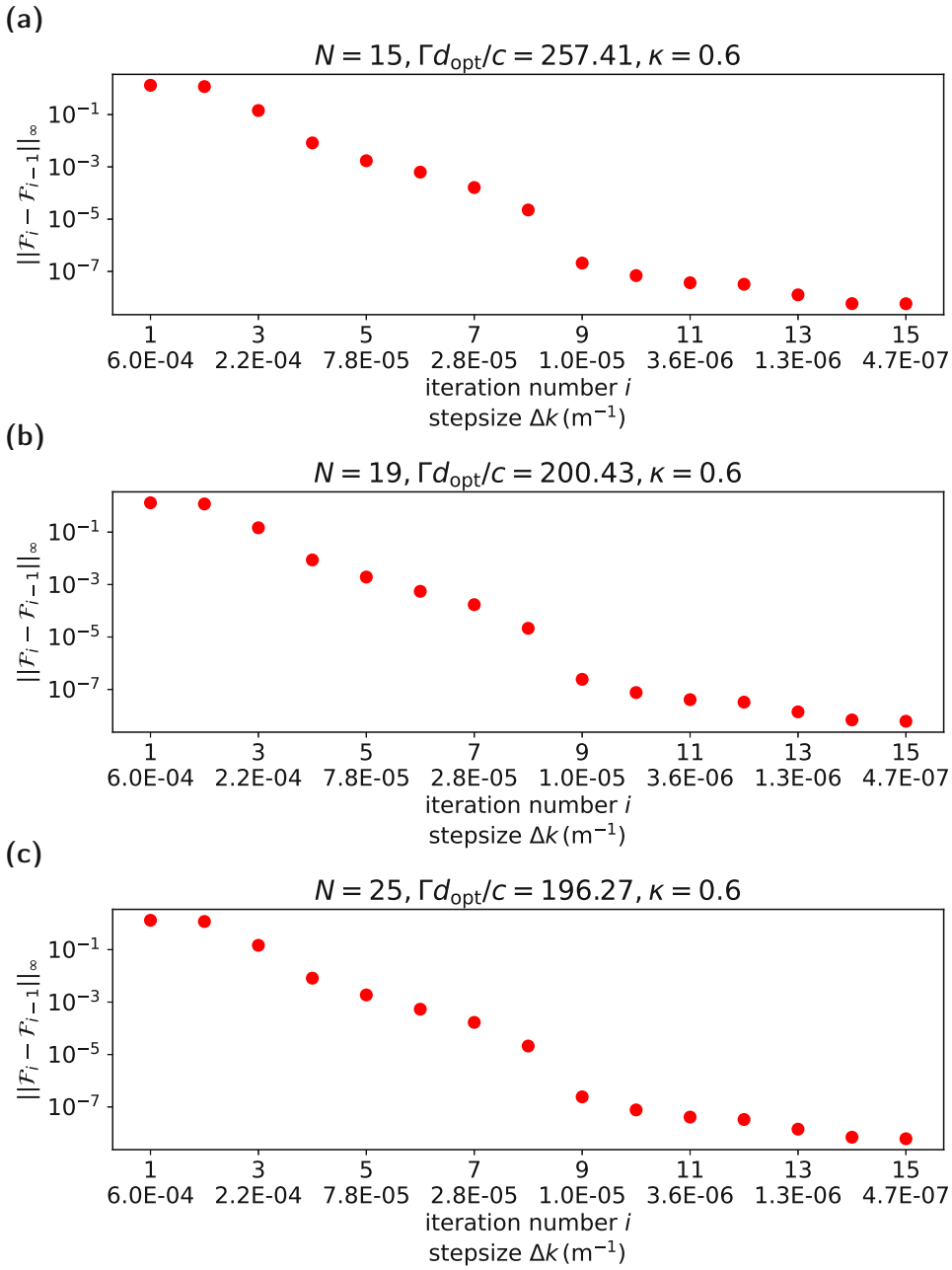

Figure A.2: Numerical convergence of the cost function for the optimal dispersion relation (see Sec. 4.2). Example results are shown for polynomial degree (a) $N = 15$, (b) $N = 19$ and (c) $N = 25$.

Appendix B

Probability Conservation

For the emission spectrum and the single-photon pulse, we want to check analytically and numerically[1], if the probability is conserved. This means, that we check, if the probabilities of the photon being in the qubit and in the waveguide, respectively, add up to one.

B.1 Emission spectrum

For the emission spectrum the probability conservation reads

$$|c_e(t)|^2 + \int_0^\infty \mathrm{d}k\, |c(k;t)|^2 = P_e(t) + \int_0^\infty \mathrm{d}k\, S(k;t) \stackrel{!}{=} 1. \tag{B.1}$$

If we integrate $S(k;t)$ over the whole k-space, we obtain the probability of the photon being inside the waveguide field at time t. The integral is given by

$$\int_0^\infty \mathrm{d}k\, S(k;t) = \int_0^\infty \mathrm{d}k\, \frac{g_0^2}{(\Gamma/2)^2 + \Delta^2} \left[1 + e^{-\Gamma t} - 2e^{-\Gamma t/2}\cos(\Delta t)\right]. \tag{B.2}$$

For this integrand, we cannot perform contour integration together with the residue theorem, except for the linear case, i.e. $\omega(k) = ck$[2]. For the latter, we can again use the fact, that $\Gamma \ll \omega_\mathrm{q}$, to write

$$\begin{aligned}\int_0^\infty \mathrm{d}k\, S(k;t) &= \int_0^\infty \mathrm{d}k\, \frac{g_0^2}{(\Gamma/2)^2 + \Delta^2} \left[1 + e^{-\Gamma t} - 2e^{-\Gamma t/2}\cos(\Delta t)\right] \\ &\approx \int_{-\infty}^{+\infty} \mathrm{d}k\, \frac{g_0^2}{(\Gamma/2)^2 + \Delta^2} \left[1 + e^{-\Gamma t} - 2e^{-\Gamma t/2}\cos(\Delta t)\right],\end{aligned}$$

where $\Delta \equiv ck - \omega_\mathrm{q}$. Analytically, we find that

$$\int_0^\infty \mathrm{d}k\, S(k;t) = \frac{2\pi g_0^2}{c\Gamma}\left(1 - e^{-\Gamma t}\right) = 1 - e^{-\Gamma t}. \tag{B.3}$$

[1] For the single-photon pulse, it is sufficient to only check the probability conservation analytically, because the pulse depends also on the $c(k;t)$, for which we already perform the numerical analysis when checking the probability conservation for the spectrum.

[2] This is due to terms of higher order in k occurring in the exponential $e^{i\omega(k)t}$.

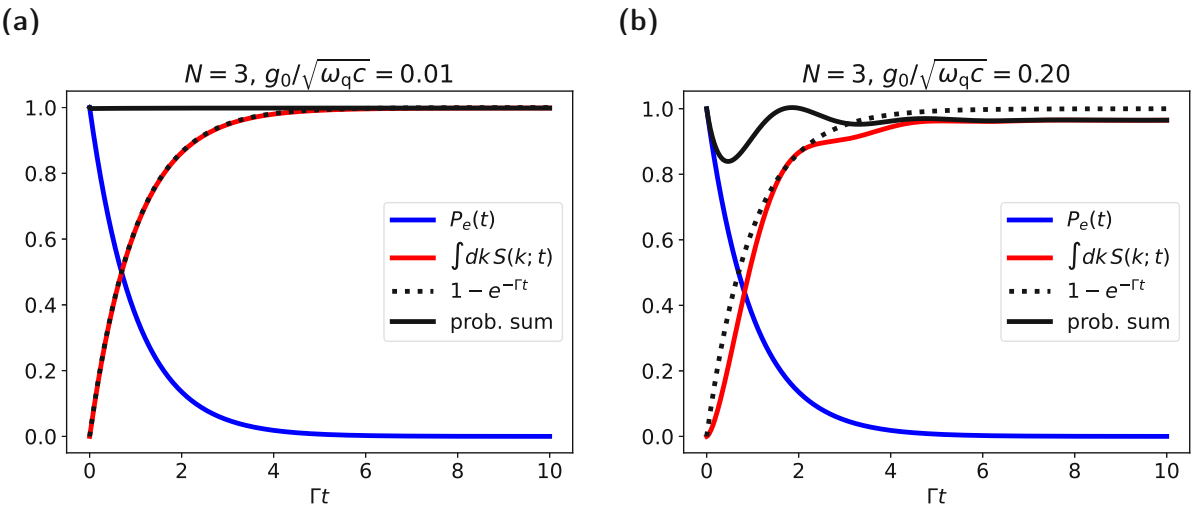

Figure B.1: Probability conservation as a function of time for a coupling strength of (a) $g_0/\sqrt{\omega_q c} = 0.01$ and (b) $g_0/\sqrt{\omega_q c} = 0.2$. Results are shown for the optimal dispersion relation of degree $N = 3$ (see Sec. 4.1).

Subsequently, Eq. (B.1) becomes

$$P_e(t) + \int_0^\infty \mathrm{d}k\, S(k;t) = e^{-\Gamma t} + 1 - e^{-\Gamma t} = 1. \tag{B.4}$$

This simply means, that for all times t, the probabilities of finding the photon in the qubit and in the field, sum up to one. The probability is conserved.

Numerically, we check, if Eq. (B.1) holds in general, i.e. if the probability is conserved also for a non-linear dispersion.

In Figs. B.1 and B.2, we plot the probability conservation as a function of time for the coupling strengths $g_0/\sqrt{\omega_q c} = 0.01$ and $g_0/\sqrt{\omega_q c} = 0.2$ for polynomial degree $N = 3$ and $N = 25$, respectively. We observe, that for $g_0/\sqrt{\omega_q c} = 0.2$, the probability conservation is not fulfilled, especially for degree $N = 25$, while for $g_0/\sqrt{\omega_q c} = 0.01$ the probability conservation is fulfilled to a good degree for all times up to $\Gamma t = 10$, where the pulse is almost fully emitted into the waveguide field and the spectrum subsequently has almost reached its final form.

In Tabs. B.1 and B.2, we show the numerical probability conservation results for the same degrees and coupling strengths as in Figs. B.1 and B.2.

For $N = 3$ (see Tab. B.1), we observe, that for small times $\Gamma t \leq 1$, the probability conservation is not fulfilled up to an absolute error of several percent for higher coupling strengths $g_0/\sqrt{\omega_q c} \geq 0.1$. For larger times $\Gamma t \geq 5$, the coupling strengths $g_0/\sqrt{\omega_q c} \geq 0.2$ still lead to large deviations from unity. This is due to the left tail of the Lorentzian getting cut by the lower integration limit $k = 0$, because the FWHM ($\Gamma \propto g_0^2$) is too big in these cases. That way, we are leaving the Markov regime. For all times, coupling strengths of $g_0/\sqrt{\omega_q c} \leq 0.05$ yield an absolute error of around 0.2% or less.

For $N = 25$ (see Tab. B.2), we observe, that for all times, the probability sum is off by an absolute error of several percent for coupling strengths $g_0/\sqrt{\omega_q c} \geq 0.05$. This is either

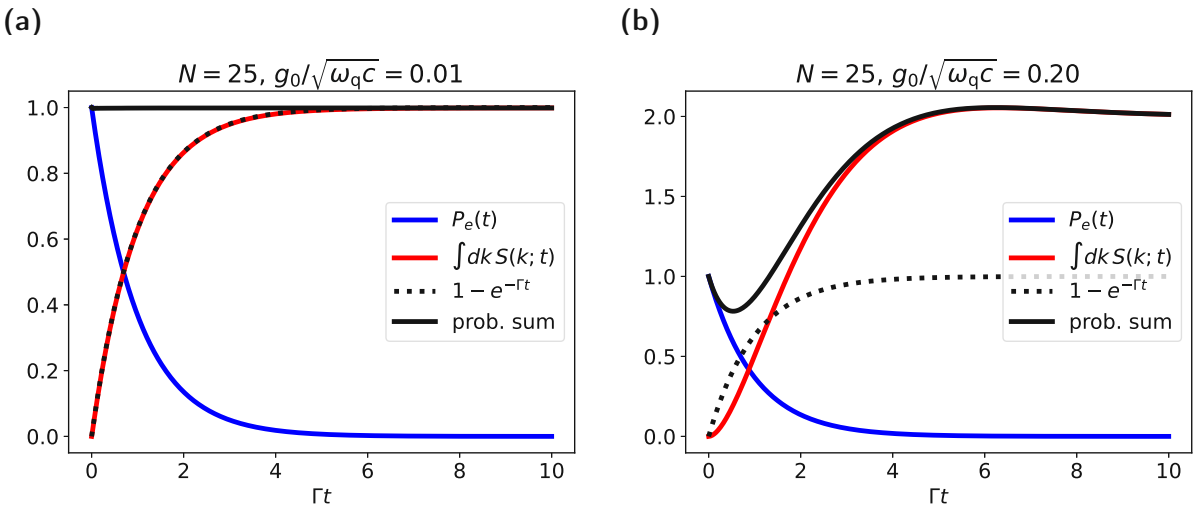

Figure B.2: Probability conservation as a function of time for a coupling strength of (a) $g_0/\sqrt{\omega_q c} = 0.01$ and (b) $g_0/\sqrt{\omega_q c} = 0.2$. Results are shown for the optimal dispersion relation of degree $N = 25$ (see Sec. 4.2).

caused by the cutting of the Lorentzian at $k = 0$ or the formation of secondary peaks for higher polynomial degrees. The latter leads to a probability sum greater than one. For all times, the coupling strength $g_0/\sqrt{\omega_q c} = 0.01$ shows acceptable probability conservation, it yields probability sums below one within an absolute error of under 0.2%. Subsequently, for all numerical calculations, we choose $g_0/\sqrt{\omega_q c} = 0.01$, such that Eq. (B.1) is fulfilled within an absolute error of $\approx 0.2\%$ for all times and also for high polynomial degrees.

B.2 Single-photon pulse

For the single-photon pulse the probability conservation reads

$$P_e(t) + \int_{-\infty}^{+\infty} \mathrm{d}x\, n(x;t) \stackrel{!}{=} 1. \tag{B.5}$$

Integrating the pulse result for a linear dispersion [see Eq. (2.43)] over all possible x yields

$$\begin{aligned}\int_{-\infty}^{+\infty} \mathrm{d}x\, n(x;t) &= \frac{\Gamma}{c}\int_0^{ct} \mathrm{d}x\, e^{-\Gamma(ct-x)/c} \\ &= \frac{\Gamma}{c} e^{-\Gamma t}\int_0^{ct} \mathrm{d}x\, e^{\Gamma x/c} \\ &= 1 - e^{-\Gamma t}.\end{aligned}$$

Subsequently, Eq. (B.5) becomes

$$P_e(t) + \int_{-\infty}^{+\infty} \mathrm{d}x\, n(x;t) = e^{-\Gamma t} + 1 - e^{-\Gamma t} = 1, \tag{B.6}$$

which verifies, that the probability is conserved.

$g_0/\sqrt{\omega_q c}$	Γ/ω_q	Γt	prob. Σ	$1-$ prob. Σ in %
0.50	1.5708	0.5	0.6829	31.7054
0.20	0.2513	0.5	0.8396	16.0393
0.10	0.0628	0.5	1.0131	-1.3137
0.05	0.0157	0.5	1.0001	-0.0085
0.02	0.0025	0.5	0.9979	0.2138
0.01	0.0006	0.5	0.9975	0.2518
0.50	1.5708	1	0.5524	44.7559
0.20	0.2513	1	0.9135	8.6500
0.10	0.0628	1	0.9905	0.9459
0.05	0.0157	1	0.9992	0.0814
0.02	0.0025	1	0.9982	0.1815
0.01	0.0006	1	0.9979	0.2147
0.50	1.5708	5	0.6018	39.8203
0.20	0.2513	5	0.9694	3.0648
0.10	0.0628	5	0.9949	0.5110
0.05	0.0157	5	0.9990	0.1036
0.02	0.0025	5	0.9987	0.1330
0.01	0.0006	5	0.9984	0.1585
0.50	1.5708	10	0.6255	37.4504
0.20	0.2513	10	0.9651	3.4874
0.10	0.0628	10	0.9949	0.5076
0.05	0.0157	10	0.9990	0.1040
0.02	0.0025	10	0.9987	0.1321
0.01	0.0006	10	0.9984	0.1575

Table B.1: Numerical probability conservation for the optimal dispersion relation of polynomial degree $N = 3$ (see Sec. 4.1) for different coupling strengths g_0 and times t.

$g_0/\sqrt{\omega_q c}$	Γ/ω_q	Γt	prob. Σ	$1-$ prob. Σ in %
0.50	1.5708	0.5	0.6436	35.6404
0.20	0.2513	0.5	0.7829	21.7124
0.10	0.0628	0.5	1.1795	-17.9483
0.05	0.0157	0.5	1.7443	-74.4336
0.02	0.0025	0.5	1.0078	-0.7816
0.01	0.0006	0.5	0.9981	0.1916
0.50	1.5708	1	0.4737	52.6334
0.20	0.2513	1	0.8740	12.6020
0.10	0.0628	1	1.8790	-87.8959
0.05	0.0157	1	1.5704	-57.0432
0.02	0.0025	1	1.0088	-0.8773
0.01	0.0006	1	0.9984	0.1625
0.50	1.5708	5	0.4790	52.0971
0.20	0.2513	5	2.0271	-102.7067
0.10	0.0628	5	2.0764	-107.6381
0.05	0.0157	5	1.3286	-32.8593
0.02	0.0025	5	1.0074	-0.7441
0.01	0.0006	5	0.9988	0.1181
0.50	1.5708	10	0.5353	46.4674
0.20	0.2513	10	2.0128	-101.2750
0.10	0.0628	10	2.0246	-102.4606
0.05	0.0157	10	1.3252	-32.5186
0.02	0.0025	10	1.0073	-0.7259
0.01	0.0006	10	0.9988	0.1173

Table B.2: Numerical probability conservation for the optimal dispersion relation of polynomial degree $N = 25$ (see Sec. 4.2) for different coupling strengths g_0 and times t.

Appendix C

Discretization of the Equations of Motion

In order to use ED to verify the pulse overlap method results, we need to discretize the EOMs of the two-qubit system. The original EOMs for two qubits read [see Eqs. (2.7)-(2.8)]

$$\dot{c}_{1,2}(t) = -i\omega_{\mathrm{q}} c_{1,2}(t) - i \int_0^\infty \mathrm{d}k \, g_{1,2}(k) c(k;t), \tag{C.1}$$

$$\dot{c}(k;t) = -i\omega(k) c(k;t) - i \left[g_1^*(k) c_1(t) + g_2^*(k) c_2(t) \right]. \tag{C.2}$$

Discretizing in k yields

$$\dot{c}_1(t) = -i\omega_{\mathrm{q}} c_1(t) - i\Delta k \sum_{n=1}^{N} g_{1,k_n} c_{k_n}(t), \tag{C.3}$$

$$\dot{c}_2(t) = -i\omega_{\mathrm{q}} c_2(t) - i\Delta k \sum_{n=1}^{N} g_{2,k_n} c_{k_n}(t), \tag{C.4}$$

$$\dot{c}_{k_n}(t) = -i\omega_{k_n} c_{k_n}(t) - i \left[g_{1,k_n}^* c_1(t) + g_{2,k_n}^* c_2(t) \right], \tag{C.5}$$

where Δk and N are the stepsize and the number of points on the k-axis, respectively. Also, $\omega_{k_n} \equiv \omega(k_n)$ and $g_{i,k_n} \equiv g_i(k_n)$. In our model, we use the couplings,

$$g_{1,2}(k) = g_0 \, \theta(k) e^{ikx_{1,2}}, \tag{C.6}$$

where the positions of the qubits, x_i, are w.l.o.g. chosen as $x_1 = 0$, $x_2 = d$.

With this discretization, the norm is not the unit anymore

$$\int \mathrm{d}k \, |c(k;t)|^2 = 1 \rightarrow \Delta k \sum_n |c_{k_n}(t)|^2 = 1 \Rightarrow \sum_n |c_{k_n}(t)|^2 = \frac{1}{\Delta k}. \tag{C.7}$$

To compensate for this change, we introduce the transformation

$$\bar{c}_{k_n}(t) := \sqrt{\Delta k} \, c_{k_n}(t), \tag{C.8}$$

through which the norm becomes the unit again

$$\sum_n |c_{k_n}(t)|^2 = \frac{1}{\Delta k}\sum_n |\bar{c}_{k_n}(t)|^2 = \frac{1}{\Delta k} \Rightarrow \sum_n |\bar{c}_{k_n}(t)|^2 = 1. \tag{C.9}$$

The EOMs for the $\bar{c}_{k_n}(t)$ read

$$\dot{c}_1(t) = -i\omega_\mathrm{q} c_1(t) - i\sqrt{\Delta k}\sum_{n=1}^{N} g_{1,k_n}\bar{c}_{k_n}(t), \tag{C.10}$$

$$\dot{c}_2(t) = -i\omega_\mathrm{q} c_2(t) - i\sqrt{\Delta k}\sum_{n=1}^{N} g_{2,k_n}\bar{c}_{k_n}(t), \tag{C.11}$$

$$\dot{\bar{c}}_{k_n}(t) = -i\omega_{k_n}\bar{c}_{k_n}(t) - i\sqrt{\Delta k}\left[g^*_{1,k_n}c_1(t) + g^*_{2,k_n}c_2(t)\right]. \tag{C.12}$$

We can write this system of coupled differential equations as a matrix equation

$$\partial_t \begin{pmatrix} c_1(t) \\ c_2(t) \\ \bar{c}_{k_1}(t) \\ \vdots \\ \bar{c}_{k_{N-1}}(t) \\ \bar{c}_{k_N}(t) \end{pmatrix} = -i \begin{pmatrix} \omega_\mathrm{q} & 0 & \bar{g}_{1,k_1} & \cdots & \bar{g}_{1,k_{N-1}} & \bar{g}_{1,k_N} \\ 0 & \omega_\mathrm{q} & \bar{g}_{2,k_1} & \cdots & \bar{g}_{2,k_{N-1}} & \bar{g}_{2,k_N} \\ \bar{g}^*_{1,k_1} & \bar{g}^*_{2,k_1} & \omega_{k_1} & & & \\ \vdots & \vdots & & \ddots & 0 & \\ \bar{g}^*_{1,k_{N-1}} & \bar{g}^*_{2,k_{N-1}} & 0 & & \omega_{k_{N-1}} & \\ \bar{g}^*_{1,k_N} & \bar{g}^*_{2,k_N} & & & & \omega_{k_N} \end{pmatrix} \begin{pmatrix} c_1(t) \\ c_2(t) \\ \bar{c}_{k_1}(t) \\ \vdots \\ \bar{c}_{k_{N-1}}(t) \\ \bar{c}_{k_N}(t) \end{pmatrix}, \tag{C.13}$$

where $\bar{g}_{i,k_n} \equiv \sqrt{\Delta k}\, g_{i,k_n}$. If we write the above equation as

$$\partial_t \vec{c}(t) = -i\,\mathbf{M}\,\vec{c}(t), \tag{C.14}$$

the formal solution is given by

$$\vec{c}(t) = e^{-i\mathbf{M}t}\,\vec{c}(0). \tag{C.15}$$

Bibliography

[1] J.-M. Raimond and S. Haroche, *Exploring the Quantum: Atoms, Cavities, and Photons*, Vol. 82 (Oxford University Press, 2006), https://academic.oup.com/book/7346.

[2] C. Gardiner and P. Zoller, *The Quantum World of Ultra-Cold Atoms and Light Book II: The Physics of Quantum-Optical Devices*, Vol. 4 (World Scientific Publishing Company, 2015), https://www.worldscientific.com/worldscibooks/10.1142/p983#t=aboutBook.

[3] H. J. Kimble, "The quantum internet", Nature **453**, 1023–1030 (2008), https://doi.org/10.1038/nature07127.

[4] J. I. Cirac, P. Zoller, H. J. Kimble, and H. Mabuchi, "Quantum State Transfer and Entanglement Distribution among Distant Nodes in a Quantum Network", Phys. Rev. Lett. **78**, 3221–3224 (1997), https://link.aps.org/doi/10.1103/PhysRevLett.78.3221.

[5] S. Gleyzes, S. Kuhr, C. Guerlin, J. Bernu, S. Deleglise, U. Busk Hoff, M. Brune, J.-M. Raimond, and S. Haroche, "Quantum jumps of light recording the birth and death of a photon in a cavity", Nature **446**, 297–300 (2007), https://doi.org/10.1038/nature05589.

[6] A. Stute, B. Casabone, P. Schindler, T. Monz, P. O. Schmidt, B. Brandstätter, T. E. Northup, and R. Blatt, "Tunable ion–photon entanglement in an optical cavity", Nature **485**, 482–485 (2012), https://doi.org/10.1038/nature11120.

[7] T. Wilk, S. C. Webster, A. Kuhn, and G. Rempe, "Single-Atom Single-Photon Quantum Interface", Science **317**, 488–490 (2007), https://www.science.org/doi/abs/10.1126/science.1143835.

[8] O. Diekmann, D. O. Krimer, and S. Rotter, "Ultrafast Excitation Exchange in a Maxwell Fish-Eye Lens", Phys. Rev. Lett. **132**, 013602 (2024), https://link.aps.org/doi/10.1103/PhysRevLett.132.013602.

[9] A. Akimov, A Mukherjee, C. Yu, D. Chang, A. Zibrov, P. Hemmer, H Park, and M. Lukin, "Generation of single optical plasmons in metallic nanowires coupled to quantum dots", Nature **450**, 402–406 (2007), https://doi.org/10.1038/nature06230.

[10] A. Gonzalez-Tudela, D. Martin-Cano, E. Moreno, L. Martin-Moreno, C. Tejedor, and F. J. Garcia-Vidal, "Entanglement of Two Qubits Mediated by One-Dimensional Plasmonic Waveguides", Phys. Rev. Lett. **106**, 020501 (2011), https://link.aps.org/doi/10.1103/PhysRevLett.106.020501.

[11] C. Gonzalez-Ballestero, E. Moreno, and F. J. Garcia-Vidal, "Generation, manipulation, and detection of two-qubit entanglement in waveguide QED", Phys. Rev. A **89**, 042328 (2014), https://link.aps.org/doi/10.1103/PhysRevA.89.042328.

[12] J.-T. Shen and S. Fan, "Theory of single-photon transport in a single-mode waveguide. I. Coupling to a cavity containing a two-level atom", Phys. Rev. A **79**, 023837 (2009), https://link.aps.org/doi/10.1103/PhysRevA.79.023837.

[13] H. Pichler, T. Ramos, A. J. Daley, and P. Zoller, "Quantum optics of chiral spin networks", Phys. Rev. A **91**, 042116 (2015), https://link.aps.org/doi/10.1103/PhysRevA.91.042116.

[14] C. Gonzalez-Ballestero, A. Gonzalez-Tudela, F. J. Garcia-Vidal, and E. Moreno, "Chiral route to spontaneous entanglement generation", Phys. Rev. B **92**, 155304 (2015), https://link.aps.org/doi/10.1103/PhysRevB.92.155304.

[15] J. Petersen, J. Volz, and A. Rauschenbeutel, "Chiral nanophotonic waveguide interface based on spin-orbit interaction of light", Science **346**, 67–71 (2014), https://www.science.org/doi/10.1126/science.1257671.

[16] R. Mitsch, C. Sayrin, B. Albrecht, P. Schneeweiss, and A. Rauschenbeutel, "Quantum state-controlled directional spontaneous emission of photons into a nanophotonic waveguide", Nature communications **5**, 5713 (2014), https://doi.org/10.1038/ncomms6713.

[17] I. Söllner, S. Mahmoodian, S. L. Hansen, L. Midolo, A. Javadi, G. Kiršanskė, T. Pregnolato, H. El-Ella, E. H. Lee, J. D. Song, et al., "Deterministic photon–emitter coupling in chiral photonic circuits", Nature nanotechnology **10**, 775–778 (2015), https://doi.org/10.1038/nnano.2015.159.

[18] B Le Feber, N Rotenberg, and L Kuipers, "Nanophotonic control of circular dipole emission", Nature communications **6**, 6695 (2015), https://doi.org/10.1038/ncomms7695.

[19] A. B. Young, A. C. T. Thijssen, D. M. Beggs, P. Androvitsaneas, L. Kuipers, J. G. Rarity, S. Hughes, and R. Oulton, "Polarization Engineering in Photonic Crystal Waveguides for Spin-Photon Entanglers", Phys. Rev. Lett. **115**, 153901 (2015), https://link.aps.org/doi/10.1103/PhysRevLett.115.153901.

[20] P. Lodahl, S. Mahmoodian, S. Stobbe, A. Rauschenbeutel, P. Schneeweiss, J. Volz, H. Pichler, and P. Zoller, "Chiral quantum optics", Nature **541**, 473–480 (2017), https://doi.org/10.1038/nature21037.

[21] H. J. Carmichael, "Quantum trajectory theory for cascaded open systems", Phys. Rev. Lett. **70**, 2273–2276 (1993), https://link.aps.org/doi/10.1103/PhysRevLett.70.2273.

[22] M. Stobińska, G. Alber, and G. Leuchs, "Perfect excitation of a matter qubit by a single photon in free space", Europhysics Letters **86**, 14007 (2009), https://dx.doi.org/10.1209/0295-5075/86/14007.

[23] Y. L. A. Rezus, S. G. Walt, R. Lettow, A. Renn, G. Zumofen, S. Götzinger, and V. Sandoghdar, "Single-Photon Spectroscopy of a Single Molecule", Phys. Rev. Lett. **108**, 093601 (2012), https://link.aps.org/doi/10.1103/PhysRevLett.108.093601.

[24] A. Sharafiev, M. L. Juan, O. Gargiulo, M. Zanner, S. Wögerer, J. J. García-Ripoll, and G. Kirchmair, "Visualizing the emission of a single photon with frequency and time resolved spectroscopy", Quantum **5**, 474 (2021), https://doi.org/10.22331/q-2021-06-10-474.

[25] Y. Wang, J. Minář, L. Sheridan, and V. Scarani, "Efficient excitation of a two-level atom by a single photon in a propagating mode", Phys. Rev. A **83**, 063842 (2011), https://link.aps.org/doi/10.1103/PhysRevA.83.063842.

[26] S. A. Aljunid, G. Maslennikov, Y. Wang, H. L. Dao, V. Scarani, and C. Kurtsiefer, "Excitation of a Single Atom with Exponentially Rising Light Pulses", Phys. Rev. Lett. **111**, 103001 (2013), https://link.aps.org/doi/10.1103/PhysRevLett.111.103001.

[27] V. Leong, M. A. Seidler, M. Steiner, A. Cere, and C. Kurtsiefer, "Time-resolved scattering of a single photon by a single atom", Nature communications **7**, 1–5 (2016), https://doi.org/10.1038/ncomms13716.

[28] G. F. Peñas, R. Puebla, and J. J. García-Ripoll, "Improving quantum state transfer: correcting non-Markovian and distortion effects", Quantum Science and Technology **8**, 045026 (2023), https://iopscience.iop.org/article/10.1088/2058-9565/acf60a.

[29] B. Srivathsan, G. K. Gulati, A. Cerè, B. Chng, and C. Kurtsiefer, "Reversing the Temporal Envelope of a Heralded Single Photon using a Cavity", Phys. Rev. Lett. **113**, 163601 (2014), https://link.aps.org/doi/10.1103/PhysRevLett.113.163601.

[30] A. Einstein, "Zur Quantentheorie der Strahlung", Physikalische Zeitschrift **18** (1916), https://doi.org/10.1515/9783112596609-016.

[31] A. M. Fox, *Quantum Optics: An Introduction*, Vol. 15 (Oxford university press, 2006), https://global.oup.com/academic/product/quantum-optics-9780198566731?cc=at&lang=en&.

[32] V. Weisskopf and E. Wigner, "Berechnung der natürlichen Linienbreite auf Grund der Diracschen Lichttheorie", Zeitschrift für Physik **63**, 54–73 (1930), https://doi.org/10.1007/BF01336768.

[33] D. A. Steck, *Quantum and Atom Optics* (2007), https://atomoptics.uoregon.edu/~dsteck/teaching/quantum-optics/.

[34] H.-P. Breuer and F. Petruccione, *The Theory of Open Quantum Systems* (Oxford University Press, USA, 2007), https://academic.oup.com/book/27757.

[35] K. Riley, M. Hobson, and S. Bence, *Mathematical Methods for Physics and Engineering: A Comprehensive Guide* (Cambridge University Press, 2006), https://doi.org/10.1017/CBO9780511810763.

[36] P. Virtanen, R. Gommers, T. E. Oliphant, M. Haberland, T. Reddy, D. Cournapeau, E. Burovski, P. Peterson, W. Weckesser, J. Bright, S. J. van der Walt, M. Brett, J. Wilson, K. J. Millman, N. Mayorov, A. R. J. Nelson, E. Jones, R. Kern, E. Larson, C. J. Carey, İ. Polat, Y. Feng, E. W. Moore, J. VanderPlas, D. Laxalde, J. Perktold, R. Cimrman, I. Henriksen, E. A. Quintero, C. R. Harris, A. M. Archibald, A. H. Ribeiro, F. Pedregosa, P. van Mulbregt, and SciPy 1.0 Contributors, "SciPy 1.0: Fundamental Algorithms for Scientific Computing in Python", Nature Methods **17**, 10.1038/s41592-019-0686-2 (2020).

[37] D. Kraft, *A Software Package for Sequential Quadratic Programming*, Deutsche Forschungs- und Versuchsanstalt für Luft- und Raumfahrt Köln: Forschungsbericht (Wiss. Berichtswesen d. DFVLR, 1988), https://degenerateconic.com/uploads/2018/03/DFVLR_FB_88_28.pdf.

List of Figures

List of Tables